

Analytical approximations of dispersion laws and ultra-complex conductivity diagrams

A.Ya. Maltsev

Steklov Mathematical Institute of Russian Academy of Sciences

8 Gubkina St., Moscow 119333, Russia

We study the probability of the emergence of ultra-complex conductivity diagrams in conductors that satisfy the tight-binding approximation and have the simple or body-centered cubic lattice. The presence of ultra-complex conductivity diagrams allows us to observe a number of highly nontrivial effects in strong magnetic fields, however, the probability of their emergence in a given substance is quite low. In the case of the simple or body-centered cubic lattice, the leading tight-binding approximation does not allow us to estimate this probability due to the peculiarities of the spectra in this situation. To estimate this probability, we use higher-order corrections to the leading approximation, which yield more accurate analytical expressions for the electron spectra.

I. INTRODUCTION

In this paper, we consider the dispersion relations arising in crystals of cubic symmetry in the tight-binding approximation. As is well known, the electron states in crystals are determined by the energy band number and the value of the quasimomentum $\mathbf{p} \in \mathbb{R}^3$, determined up to the vectors of the reciprocal lattice L^* . The basis $(\mathbf{a}_1, \mathbf{a}_2, \mathbf{a}_3)$ of the lattice L^* is given by the relations

$$\begin{aligned} \mathbf{a}_1 &= 2\pi\hbar \frac{\mathbf{l}_2 \times \mathbf{l}_3}{(\mathbf{l}_1, \mathbf{l}_2, \mathbf{l}_3)}, & \mathbf{a}_2 &= 2\pi\hbar \frac{\mathbf{l}_3 \times \mathbf{l}_1}{(\mathbf{l}_1, \mathbf{l}_2, \mathbf{l}_3)}, \\ \mathbf{a}_3 &= 2\pi\hbar \frac{\mathbf{l}_1 \times \mathbf{l}_2}{(\mathbf{l}_1, \mathbf{l}_2, \mathbf{l}_3)}, \end{aligned}$$

where $(\mathbf{l}_1, \mathbf{l}_2, \mathbf{l}_3)$ represent the basis of the crystallographic lattice L .

Thus, all the vectors

$$\begin{aligned} \mathbf{p} &\equiv \mathbf{p} + n_1 \mathbf{a}_1 + n_2 \mathbf{a}_2 + n_3 \mathbf{a}_3, \\ n_1, n_2, n_3 &\in \mathbb{Z} \end{aligned}$$

define the same electronic state for a given energy band. As a consequence, the values of the electron quasimomentum can be considered as points on a three-dimensional torus

$$\mathbf{p} \in \mathbb{T}^3 = \mathbb{R}^3 / L^*,$$

obtained by factorizing the space \mathbb{R}^3 by the reciprocal lattice vectors.

In practice, it is actually convenient to consider both representations $\mathbf{p} \in \mathbb{T}^3$ and $\mathbf{p} \in \mathbb{R}^3$.

The dependence of the electron energy $\epsilon(\mathbf{p})$ on its quasimomentum determines the dispersion relation (dispersion law) for a given energy band in a crystal. Depending on the representation, $\epsilon(\mathbf{p})$ can be considered either a function on the torus $\mathbb{T}^3 = \mathbb{R}^3 / L^*$, or a 3-periodic function in the full space \mathbb{R}^3 .

As is well known, the greatest interest in the study of conductors is in the conduction bands, i.e., energy bands

only partially filled with electrons. It is also well known that every conductor has the Fermi level (Fermi energy) ϵ_F , separating occupied electron states from unoccupied ones. Each conduction band has its own Fermi surface

$$S_F : \quad \epsilon(\mathbf{p}) = \epsilon_F,$$

which can also be viewed either as a smooth compact surface in the torus \mathbb{T}^3 , or as a 3-periodic surface in the full \mathbf{p} -space (Fig. 1, a). Most electronic phenomena in conductors are determined by the behavior of electrons near the Fermi surface.

This work is concerned with the description of electron transport phenomena in conductors in the presence of strong magnetic fields. The presence of an external magnetic field \mathbf{B} causes the evolution of electron states in \mathbf{p} -space according to the dynamic system

$$\dot{\mathbf{p}} = \frac{e}{c} [\mathbf{v}_{\text{gr}}(\mathbf{p}) \times \mathbf{B}] \equiv \frac{e}{c} [\nabla \epsilon(\mathbf{p}) \times \mathbf{B}] \quad (\text{I.1})$$

(see for example [1–4]).

Geometrically, the trajectories of system (I.1) are defined by the intersections of planes orthogonal to \mathbf{B} , and constant energy surfaces $\epsilon(\mathbf{p}) = \text{const}$ (Fig. 1, b).

The condition for strong magnetic fields can be formally written as $\omega_B \tau \gg 1$, where $\omega_B = eB/m^*c$ is the cyclotron frequency, and τ is the electron mean free time (m^* plays the role of the effective electron mass in the crystal).

More precisely, the quantity B is sufficiently large if the electron manages to travel a sufficiently large distance (much larger than the size of the Brillouin zone) along the trajectories of system (I.1) between two scattering events. It should be noted immediately that such a situation arises only for sufficiently pure single-crystal samples at low temperatures ($T \leq 1\text{K}$) in sufficiently strong magnetic fields ($B \geq 1\text{Tl}$).

As can be seen, for sufficiently complex Fermi surfaces, the shape of the trajectories of (I.1) can also be very complex (Fig. 1, b). In particular, the trajectories of (I.1) can be both closed and open (unclosed) in the \mathbf{p} -space (and in the torus $\mathbb{T}^3 = \mathbb{R}^3 / L^*$). As was shown

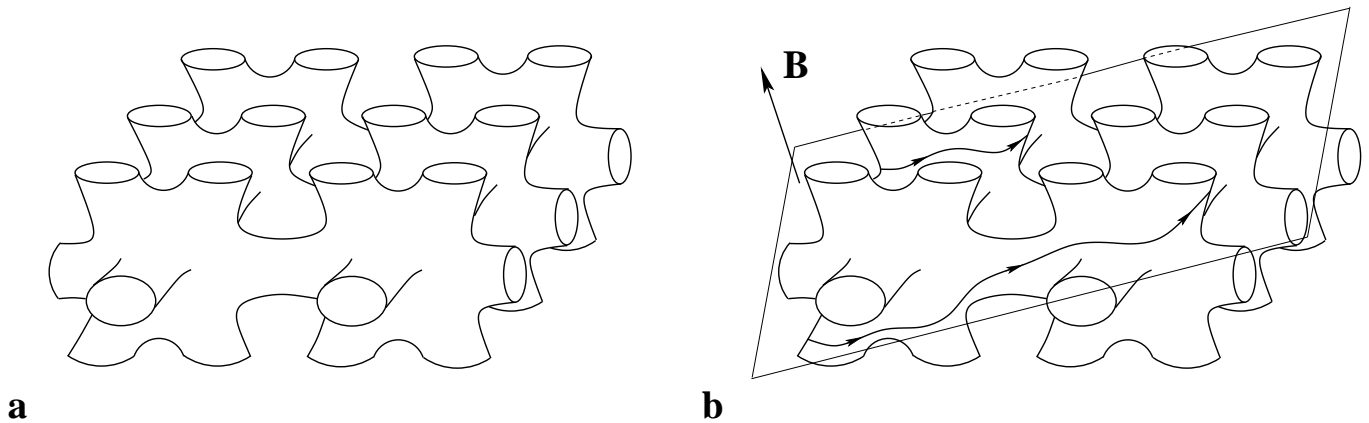


FIG. 1: (a) The Fermi surface of a complex shape in \mathbf{p} - space. (b) Trajectories of system (I.1) on the Fermi surface.

in [5–8], the behavior of electron transport phenomena in the limit $\omega_B\tau \rightarrow \infty$ strongly depends on the shape of the trajectories of (I.1) and, in particular, on the presence or absence of open trajectories on the Fermi surface.

The shape of the trajectories of (I.1) on a given Fermi surface depends significantly on the direction of \mathbf{B} . Here we will be interested in the behavior of the electrical conductivity tensor $\sigma^{kl}(\mathbf{B})$ in the limit $B \rightarrow \infty$. In view of the above, the “angular diagrams” marking the emergence of open trajectories on the Fermi surface (as well as their type) for different directions

$$\mathbf{n} = \mathbf{B}/B \in \mathbb{S}^2$$

will be very important for us.

The problem of describing all possible types of trajectories of system (I.1) (for an arbitrary dispersion relation $\epsilon(\mathbf{p})$) was set by S.P. Novikov in his paper [9]. This problem, like its numerous applications, was actively studied in his topological school (see, e.g., [10–29]). In particular, a complete classification of all possible types of open trajectories of (I.1) (as well as the corresponding behavioral regimes of the tensor $\sigma^{kl}(\mathbf{B})$ for $B \rightarrow \infty$) has now been obtained. Here we will use this classification in describing the above-mentioned angular diagrams. We will also call such diagrams angular diagrams of conductivity (of a metal) in strong magnetic fields.

For simple Fermi surfaces (Fig. 2, a, b), the angular conductivity diagrams are also very simple. Namely, each direction of \mathbf{B} corresponds to the presence of only closed trajectories (of a fairly simple shape) on the Fermi surface. The behavior of the conductivity tensor in strong magnetic fields is described by the formula ([5]):

$$\sigma_{\text{closed}}^{kl} \simeq \frac{ne^2\tau}{m^*} \begin{pmatrix} (\omega_B\tau)^{-2} & (\omega_B\tau)^{-1} & (\omega_B\tau)^{-1} \\ (\omega_B\tau)^{-1} & (\omega_B\tau)^{-2} & (\omega_B\tau)^{-1} \\ (\omega_B\tau)^{-1} & (\omega_B\tau)^{-1} & * \end{pmatrix}, \quad (\text{I.2})$$

($\omega_B\tau \rightarrow \infty$).

Formula (I.2) describes the asymptotic behavior of the components $\sigma^{kl}(\mathbf{B})$ in the limit $B \rightarrow \infty$; in particu-

lar, it is assumed that each matrix element in (I.2) has a dimensionless factor of order 1. The quantity n here represents the concentration of charge carriers in the metal (and the sign $*$ denotes a dimensionless quantity of order 1). In formula (I.2), it is also assumed that the z axis is directed along the \mathbf{B} direction.

An important remark should be made immediately, however. “Simple” Fermi surfaces can be divided into two types, namely, electron-type Fermi surfaces (Fig. 2, a) and hole-type Fermi surfaces (Fig. 2, b). Electron-type Fermi surfaces enclose regions $\epsilon(\mathbf{p}) < \epsilon_F$, while hole-type surfaces enclose regions $\epsilon(\mathbf{p}) > \epsilon_F$, which is directly reflected in the behavior of the Hall conductivity $\sigma^{xy}(\mathbf{B})$. Namely, the contribution of the electron-type Fermi surface to the Hall conductivity is given in the leading order by the formula ([1–4, 8])

$$\sigma^{xy} = -\sigma^{yx} = \frac{ec}{B} \frac{2V}{(2\pi\hbar)^3}, \quad (\text{I.3})$$

while the contribution from the hole-type Fermi surface is given by the formula

$$\sigma^{xy} = -\sigma^{yx} = -\frac{ec}{B} \frac{2V}{(2\pi\hbar)^3}, \quad (\text{I.4})$$

In formulas (I.3) - (I.4), the quantity V represents the volume bounded by the Fermi surface in \mathbf{p} - space. Note that the quantities (I.3) - (I.4) do not depend on the direction of \mathbf{B} , i.e., they are constant over the entire angular diagram for a given value of B (for “simple” Fermi surfaces).

It can also be noted that, for the relation $\epsilon(\mathbf{p})$ with the range of values

$$\epsilon_{\min} \leq \epsilon(\mathbf{p}) \leq \epsilon_{\max},$$

electron-type Fermi surfaces arise at ϵ_F close to ϵ_{\min} , and hole-type Fermi surfaces arise at ϵ_F close to ϵ_{\max} .

Periodic open trajectories (Fig. 2, c) represent the simplest open trajectories of system (I.1). Their contribution to the tensor $\sigma^{kl}(\mathbf{B})$ in the limit $\omega_B\tau \rightarrow \infty$ is

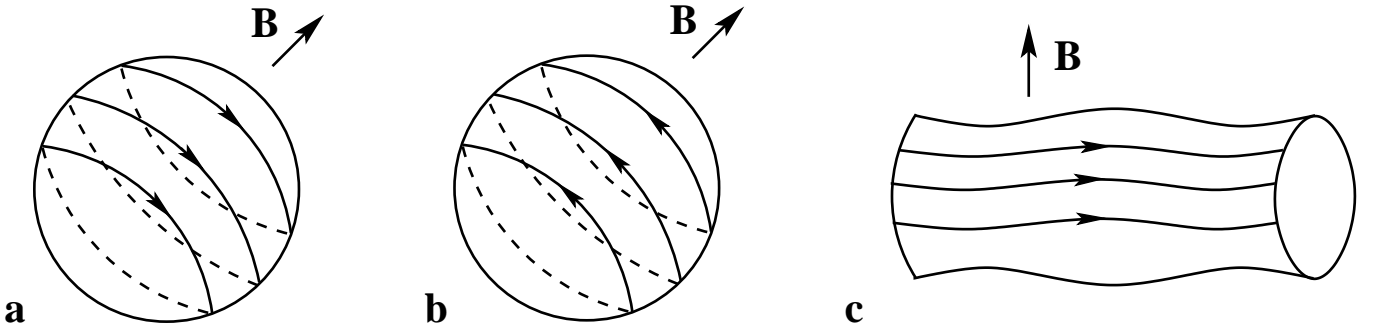


FIG. 2: (a,b) Simple Fermi surfaces of electron and hole type carrying closed trajectories of system (I.1). (c) Periodic trajectories of system (I.1).

given by the asymptotic formula ([5]):

$$\Delta\sigma_{\text{periodic}}^{kl} \simeq \frac{ne^2\tau}{m^*} \begin{pmatrix} (\omega_B\tau)^{-2} & (\omega_B\tau)^{-1} & (\omega_B\tau)^{-1} \\ (\omega_B\tau)^{-1} & * & * \\ (\omega_B\tau)^{-1} & * & * \end{pmatrix} \quad (\text{I.5})$$

In formula (I.5), as in formula (I.2), the z axis is directed along the magnetic field \mathbf{B} . Moreover, in formula (I.5) the direction of the x axis coincides with the mean direction of the open trajectories in \mathbf{p} -space. It is easy to see that the main difference between formula (I.5) and formula (I.2) is the emergence of strong anisotropy of conductivity in the plane orthogonal to \mathbf{B} . Note also that when open trajectories appear on the Fermi surface, formulas (I.3) - (I.4) cease to be satisfied.

It can be seen that the periodic trajectories shown in Fig. 2, c, are stable for small rotations of \mathbf{B} in the plane orthogonal to their mean direction, and are destroyed for other rotations of \mathbf{B} . The emergence of such trajectories on the Fermi surface thus corresponds to one-dimensional segments on the angular diagram (i.e., on the sphere $\mathbb{S}^2 \ni \mathbf{n} = \mathbf{B}/B$).

It is easy to see that the emergence of open trajectories of system (I.1) is possible only on sufficiently complex Fermi surfaces. In general, the complexity of a Fermi surface is characterized by its genus g , as well as its topological rank $\text{Rank } S_F$.

The genus of the Fermi surface is related to its representation as a compact (orientable) surface

$$S_F \subset \mathbb{T}^3 = \mathbb{R}^3/L^* ,$$

embedded in a three-dimensional torus. In this representation, the Fermi surface is homeomorphic to one of the canonical surfaces (Fig. 3, a), determined by the value g . The genus of the Fermi surface can take the values $g = 0, 1, 2, 3, 4, \dots$

The rank of the Fermi surface is related to the features of its embedding in \mathbb{T}^3 and \mathbb{R}^3 and is equal to the number of independent directions in which it extends in \mathbf{p} -space (Fig. 3, b). The rank of the Fermi surface can take values 0, 1, 2, and 3.

It is easy to see that the Fermi surfaces shown in Fig. 2, a, b, have genus $g = 0$ and $\text{Rank } S_F = 0$, while the Fermi surface shown in Fig. 2, c, has genus $g = 1$ and $\text{Rank } S_F = 1$. Here we will be interested in more complicated Fermi surfaces, having genus $g \geq 3$ and $\text{Rank } S_F = 3$.

The main type of open trajectories of system (I.1) are stable open trajectories, i.e. trajectories that are preserved and do not change their shape significantly under small rotations of \mathbf{B} , as well as variations in the level ϵ_F . According to [10, 11, 13], stable open trajectories of (I.1) have remarkable properties. Namely:

- 1) Each stable open trajectory of (I.1) lies in a straight strip of finite width (in a plane orthogonal to \mathbf{B}), passing through it (Fig. 4).
- 2) The mean direction of stable open trajectories in \mathbf{p} -space is given by the intersection of the plane orthogonal to \mathbf{B} and some integer (generated by two reciprocal lattice vectors) plane Γ , which is unchanged under small rotations of \mathbf{B} .

The contribution of stable open trajectories to the tensor $\sigma^{kl}(\mathbf{B})$ is also strongly anisotropic in the plane orthogonal to \mathbf{B} and is described by the formula (I.5) in the leading order at $B \rightarrow \infty$. This property is particularly convenient for the experimental study of such trajectories and, in particular, played an important role in the introduction of topological numbers observable in the conductivity of normal metals in the work [18].

The emergence of stable open trajectories on the Fermi surface corresponds to two-dimensional regions $\Omega_\alpha \subset \mathbb{S}^2$ (Stability Zones) on the angular diagram, each of which corresponds to its own integer plane Γ_α . As is easy to see, the emergence of stable open trajectories is possible only on sufficiently complex Fermi surfaces (like Fig. 1).

Angular diagrams containing Stability Zones Ω_α arise in the energy range

$$\epsilon_F \in (\epsilon_1^A, \epsilon_2^A) ,$$

narrower than the full range of values of $\epsilon(\mathbf{p})$:

$$\epsilon_{\min} \leq \epsilon_1^A < \epsilon_2^A \leq \epsilon_{\max}$$

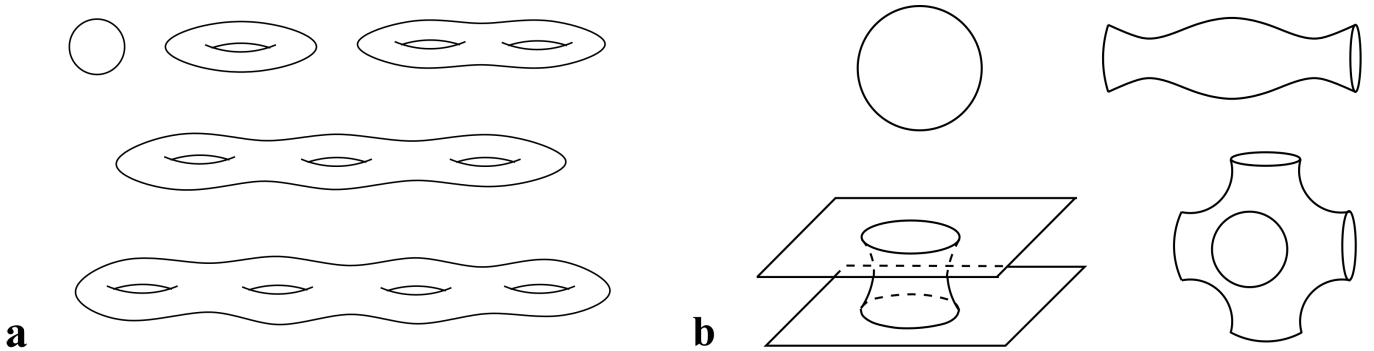


FIG. 3: (a) Abstract Fermi surfaces of genus 0, 1, 2, 3, and 4. (b) Fermi surfaces of rank 0, 1, 2, and 3.

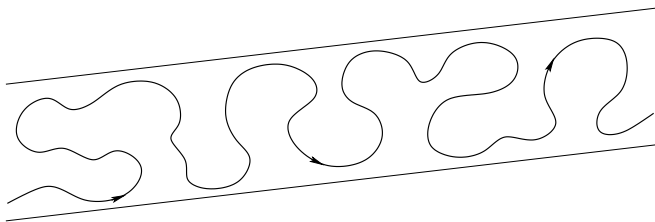


FIG. 4: The shape of a stable open trajectory of system (I.1) in a plane orthogonal to \mathbf{B} (schematically).

We will call such diagrams complex conductivity diagrams.

In fact, the interval $(\epsilon_1^A, \epsilon_2^A)$ has an additional structure associated, among other things, with the behavior of Hall conductivity in strong magnetic fields ([27, 28]). Namely, in the general case, the interval $(\epsilon_1^A, \epsilon_2^A)$ can be divided into 3 intervals

$$(\epsilon_1^A, \epsilon_2^A) = (\epsilon_1^A, \epsilon_1^B) \cup [\epsilon_1^B, \epsilon_2^B] \cup (\epsilon_2^B, \epsilon_2^A),$$

corresponding to different types of complex angular diagrams.

For values $\epsilon_F \in (\epsilon_1^A, \epsilon_1^B)$ the conductivity diagrams (diagrams of type A_-) contain a finite number of Stability Zones (Fig. 5, a). Most of the diagram, as a rule, is filled with directions \mathbf{B} , corresponding to the presence of only closed trajectories on the Fermi surface. For all such directions \mathbf{B} the Hall conductivity is of the electron type, and one can use the relation

$$\sigma^{xy} = -\sigma^{yx} = \frac{ec}{B} \frac{2V_-}{(2\pi\hbar)^3}, \quad (\text{I.6})$$

where V_- is the volume of the region $\epsilon(\mathbf{p}) < \epsilon_F$ in the torus $\mathbb{T}^3 = \mathbb{R}^3/L^*$. It can be seen that the Hall conductivity has the same value (for a given value of B) in this part of the angular diagram.

Similarly, for $\epsilon_F \in (\epsilon_2^B, \epsilon_2^A)$ the conductivity diagrams (diagrams of type A_+) contain a finite number of Stability Zones (Fig. 5, b). Most of the diagram also corresponds to the presence of only closed trajectories on the

Fermi surface. The Hall conductivity in this part is of the hole type and is given by the relation

$$\sigma^{xy} = -\sigma^{yx} = -\frac{ec}{B} \frac{2V_+}{(2\pi\hbar)^3}, \quad (\text{I.7})$$

where V_+ is the volume of the region $\epsilon(\mathbf{p}) > \epsilon_F$ in the torus $\mathbb{T}^3 = \mathbb{R}^3/L^*$.

The diagrams of type A_- and A_+ are separated by even more complex diagrams (diagrams of type B), which we will call ultra-complex conductivity diagrams (Fig. 6).

In the generic case, diagrams of type B arise in a finite energy interval $[\epsilon_1^B, \epsilon_2^B]$ ([27, 28]), separating the intervals $(\epsilon_1^A, \epsilon_1^B)$ and $(\epsilon_2^B, \epsilon_2^A)$. Generic type B diagrams contain an infinite number of zones Ω_α , and among the regions corresponding to the presence of only closed trajectories on the Fermi surface, there are both regions of electron and hole Hall conductivity (Fig. 6). As before, in regions of the first type, one can use the formula (I.6), and in regions of the second type, the formula (I.7).

Accumulation points of small Zones Ω_α typically correspond to the emergence of complex “chaotic” trajectories (of the Tsarev or Dynnikov type) on the Fermi surface. The most complex of these (Dynnikov-type trajectories) have a very complex shape, “wandering everywhere” in planes orthogonal to \mathbf{B} (Fig. 7, a).

The complex shape of such trajectories is also reflected in their contribution to the conductivity tensor in the limit $B \rightarrow \infty$ (suppression of conductivity along the direction of \mathbf{B} , the emergence of fractional powers of $\omega_B\tau$ in the components $\sigma^{kl}(\mathbf{B})$, etc. [19, 25]). We also note here that numerous properties of chaotic trajectories in general are of great interest and are actively studied at the present time (see [29–43]).

It can also be noted that the diminishing of the Zones Ω_α is accompanied by a complication of the shape of stable open trajectories (Fig. 7, b) and a complication of their contribution to the tensor $\sigma^{kl}(\mathbf{B})$, gradually transferring them to the “chaotic” regime.

Although the occurrence of type B diagrams is a general property of generic dispersion laws, they have not yet been observed experimentally. In our opinion, this is

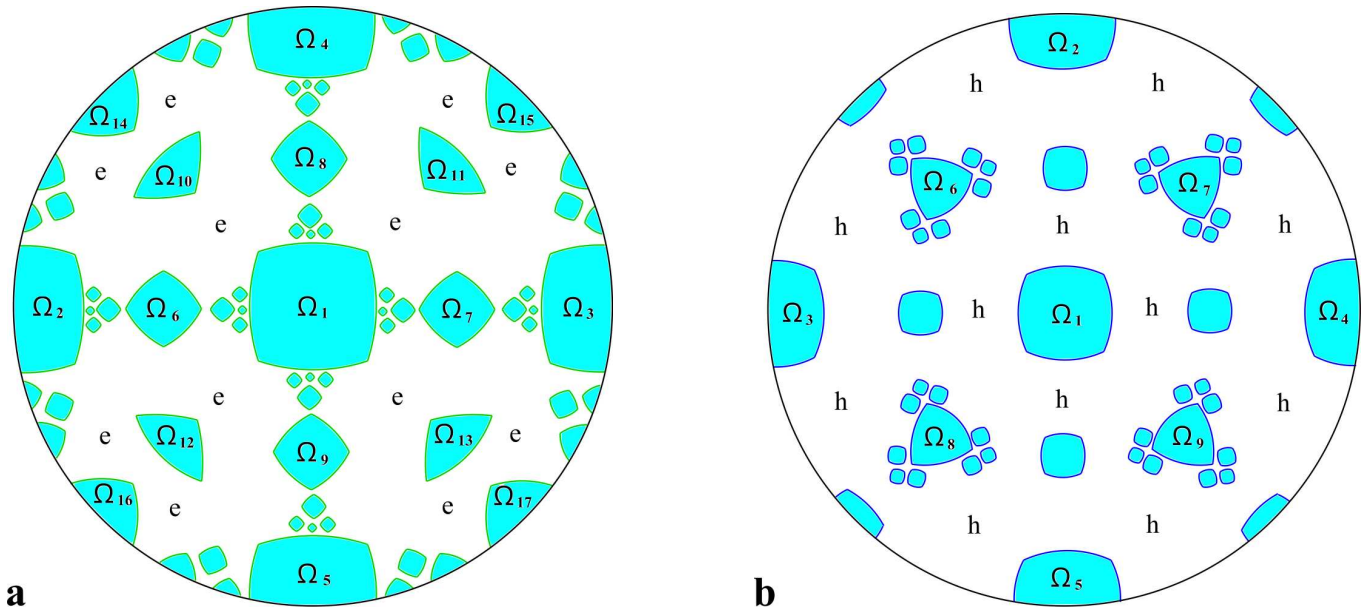


FIG. 5: (a) Complex angular diagram of type A_- (schematically). (b) Complex angular diagram of type A_+ (schematically). (The signs e and h denote the type of Hall conductivity in regions where only closed trajectories are present on the Fermi surface.)

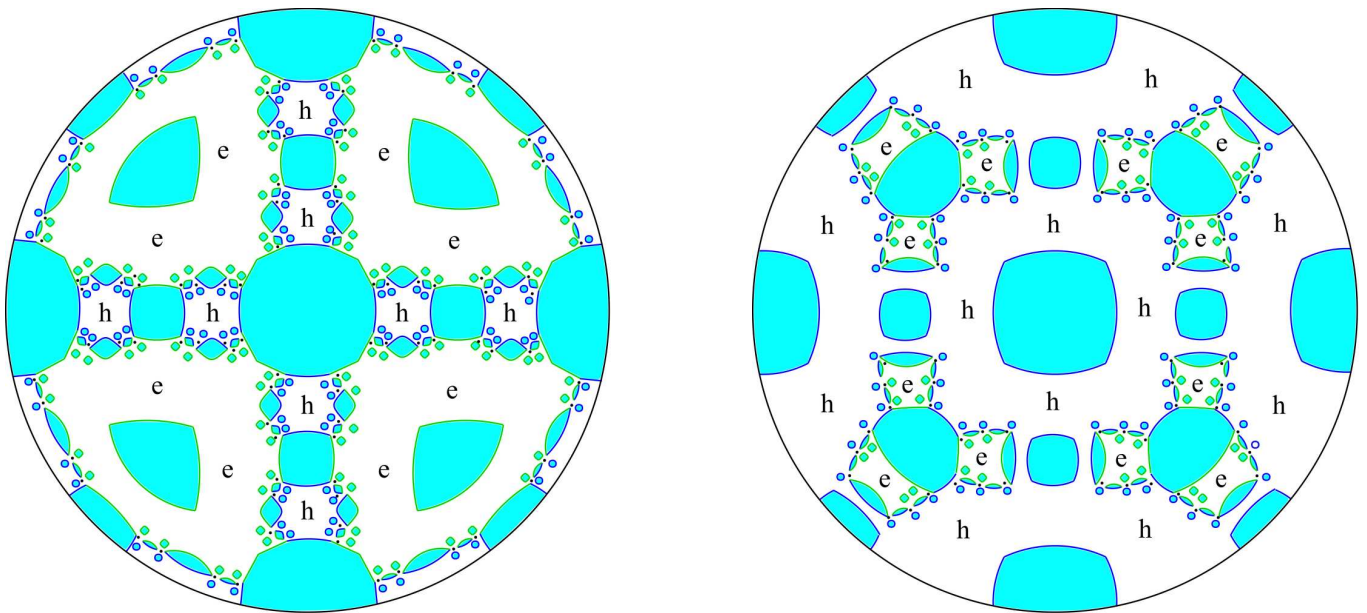


FIG. 6: Type B diagrams (schematically). The signs e and h denote the type of Hall conductivity in regions where only closed trajectories are present on the Fermi surface.

due to the extreme narrowness of the interval $[\epsilon_1^B, \epsilon_2^B]$ for real dispersion laws. In this paper, we estimate the position of the interval $[\epsilon_1^B, \epsilon_2^B]$ and its width for analytical relations $\epsilon(\mathbf{p})$ based on the tight-binding approximation for crystals with cubic symmetry.

The paper [44] contains estimates for the position of the interval $[\epsilon_1^B, \epsilon_2^B]$ for the simple, face-centered, and

body-centered cubic lattices in the leading order of the tight-binding approximation. It should be noted, however, that the leading order of the tight-binding approximation does not allow one to estimate the width of the interval $[\epsilon_1^B, \epsilon_2^B]$ for the simple and body-centered lattices and determines only its position ($\epsilon_F \simeq 0$). The reason for this is that the leading order of the tight-binding ap-

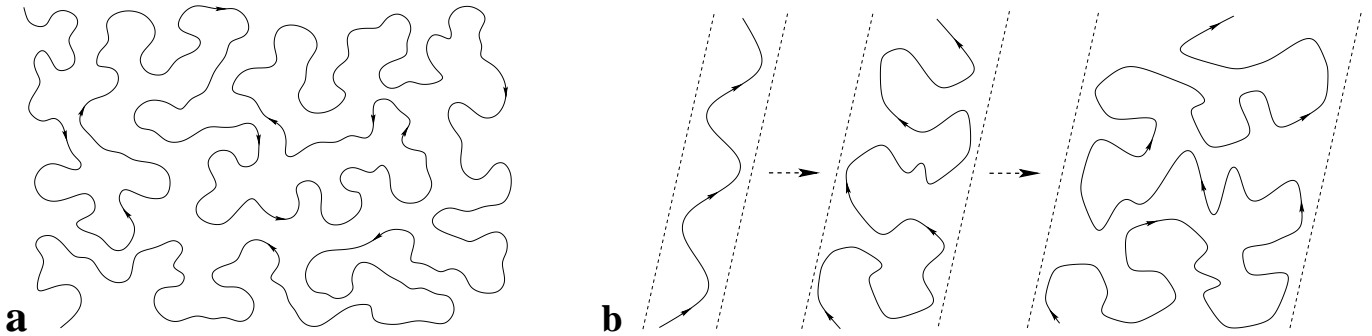


FIG. 7: (a) Chaotic trajectory of the Dynnikov type in a plane orthogonal to \mathbf{B} (schematically). (b) Increasing complexity of the shape of stable open trajectories with decreasing sizes of the Zones Ω_α .

proximation gives here non-generic dispersion relations $\epsilon(\mathbf{p})$ with the intervals $[\epsilon_1^{\mathcal{B}}, \epsilon_2^{\mathcal{B}}]$ contracted to a point ($\epsilon_1^{\mathcal{B}} = \epsilon_2^{\mathcal{B}}$).

The property described above is, in fact, inherent in all dispersion relations $\epsilon(\mathbf{p})$ that contain only odd Fourier harmonics, such that

$$\epsilon\left(\mathbf{p} + \frac{1}{2}(\mathbf{a}_1 + \mathbf{a}_2 + \mathbf{a}_3)\right) = -\epsilon(\mathbf{p})$$

In particular, this applies to the dispersion relation

$$\epsilon(\mathbf{p}) \sim \cos \frac{p_x l}{\hbar} + \cos \frac{p_y l}{\hbar} + \cos \frac{p_z l}{\hbar},$$

arising in the leading order of the tight-binding approximation for the simple cubic lattice. The Fermi surface

$$\cos \frac{p_x l}{\hbar} + \cos \frac{p_y l}{\hbar} + \cos \frac{p_z l}{\hbar} = 0$$

contains open trajectories of (I.1) for any direction of \mathbf{B} ([15]), and the corresponding angular diagram has the most complex form (being completely filled with Zones Ω_α , as well as “chaotic” and “special rational” directions of \mathbf{B} [15, 26, 29]). For $\epsilon_F < 0$ the angular conductivity diagrams are of type A_- (or belong to the class of simple ones), and for $\epsilon_F > 0$ - of type A_+ (or belong to the class of simple ones).

A similar situation also arises in the case of a body-centered cubic lattice, where the dispersion relation in the leading order has the form

$$\epsilon(\mathbf{p}) \sim \cos \frac{p_x l}{\hbar} \cos \frac{p_y l}{\hbar} \cos \frac{p_z l}{\hbar}$$

In this paper, we estimate the width of the interval $[\epsilon_1^{\mathcal{B}}, \epsilon_2^{\mathcal{B}}]$ for the simple and body-centered cubic lattices, taking into account higher-order corrections in the tight-binding approximation. The corrections to the leading term are given here by the higher Fourier harmonics determined by the lattice geometry. From the general point of view, the corresponding dispersion laws are a special case of analytic dispersion relations, which are also widely

considered in the literature (see, e.g., [6–8]). In the next chapter, we briefly describe a simplified method for estimating the position of the interval $[\epsilon_1^{\mathcal{B}}, \epsilon_2^{\mathcal{B}}]$ and also carry out this estimate for the simple cubic lattice. In Chapter 3, we will estimate the position of $[\epsilon_1^{\mathcal{B}}, \epsilon_2^{\mathcal{B}}]$ for the body-centered lattice, where the Fermi surfaces have a more complex geometry.

II. METHODS FOR ESTIMATING THE INTERVAL $[\epsilon_1^{\mathcal{B}}, \epsilon_2^{\mathcal{B}}]$ AND THE CASE OF THE SIMPLE CUBIC LATTICE

To find the interval $[\epsilon_1^{\mathcal{B}}, \epsilon_2^{\mathcal{B}}]$, it is necessary to study the system (I.1) on the Fermi surfaces $\epsilon(\mathbf{p}) = \epsilon_F$ for various values of ϵ_F . In fact, angular diagrams similar to those for the Fermi surfaces can be constructed for the entire dispersion law ([17]). Such angular diagrams contain Stability Zones W_α , which now form an everywhere dense set on the sphere \mathbb{S}^2 (Fig. 8, a). Each of the Zones Ω_α is a subregion of some Zone W_α , corresponding to the same integer plane Γ_α .

For each $\mathbf{n} = \mathbf{B}/B \in \Omega_\alpha$ system (I.1) has a certain structure on the corresponding Fermi surface ([10, 13, 17]). Namely, the Fermi surface contains a certain number of cylinders of closed trajectories dividing it into “carriers of open trajectories”, which, in turn, are periodically deformed integer planes (with holes) in \mathbf{p} -space (Fig. 9, a). At the boundary of a Zone Ω_α the described structure of trajectories is destroyed due to the vanishing of the height of one of the cylinders of closed trajectories separating the carriers of open trajectories (Fig. 9, b).

For $\mathbf{n} \in W_\alpha$ a similar structure of system (I.1) is preserved in a certain interval

$$\epsilon_F \in [\tilde{\epsilon}_1(\mathbf{n}), \tilde{\epsilon}_2(\mathbf{n})],$$

where $\tilde{\epsilon}_1(\mathbf{n})$ and $\tilde{\epsilon}_2(\mathbf{n})$ are some continuous functions on the sphere \mathbb{S}^2 ([17]), such that

$$\tilde{\epsilon}_1(\mathbf{n}) \leq \tilde{\epsilon}_2(\mathbf{n})$$

(i.e. at every point of the sphere).

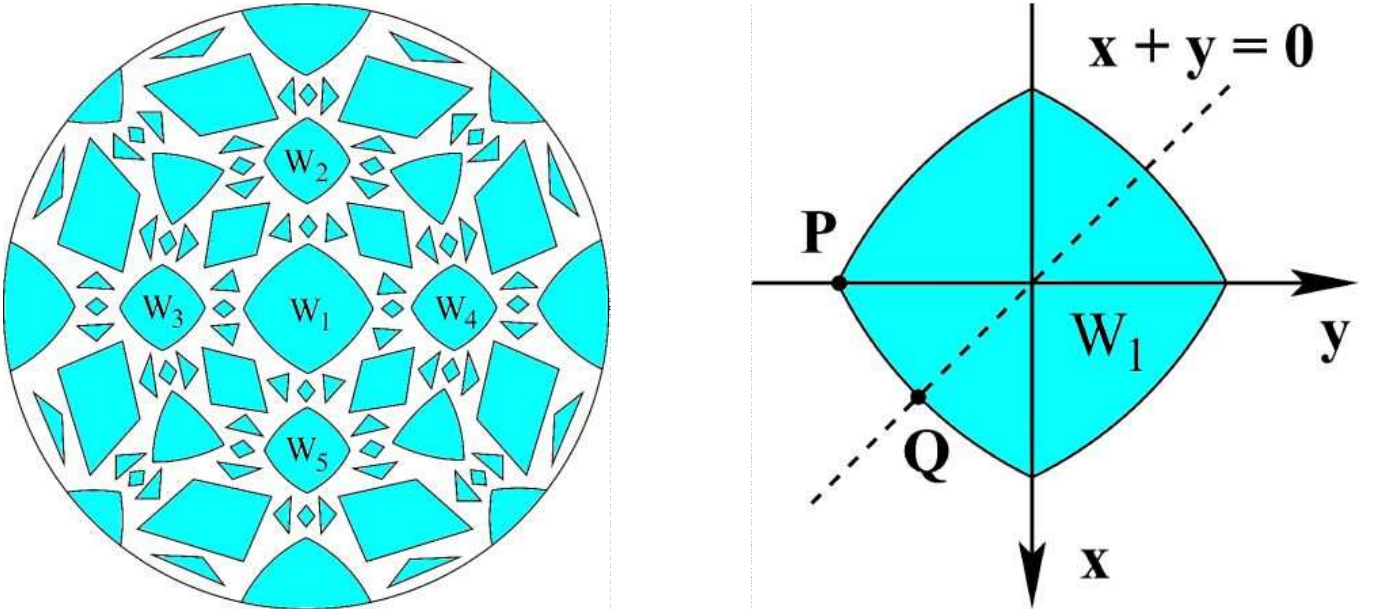


FIG. 8: (a) Zones W_α on the “full” angular diagram for a dispersion relation $\epsilon(\mathbf{p})$. (b) “Symmetric” points P and Q on the boundary of the symmetric Zone W_1 .

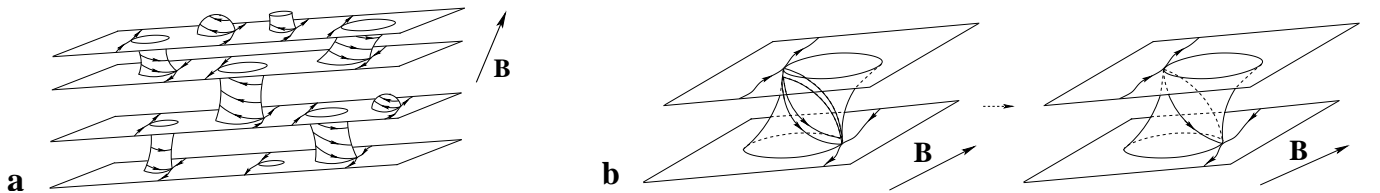


FIG. 9: (a) Complex Fermi surface divided by closed trajectories into carriers of open trajectories. (b) Vanishing of the height of a cylinder of closed trajectories at the boundary of a Zone Ω_α or W_α .

The boundary of a Zone W_α is determined by the disappearance of at least two cylinders of closed trajectories (electron and hole types) separating the carriers of open trajectories. This condition generally determines both the position of the boundary of W_α and the value of the function

$$\tilde{\epsilon}_0(\mathbf{n}) = \tilde{\epsilon}_1(\mathbf{n}) = \tilde{\epsilon}_2(\mathbf{n})$$

for $\mathbf{n} \in \partial W_\alpha$ ([17]).

According to [27, 28], the quantities $\epsilon_1^{\mathcal{B}}$ and $\epsilon_2^{\mathcal{B}}$ satisfy the relations

$$\epsilon_1^{\mathcal{B}} = \min_{\mathbb{S}^2} \tilde{\epsilon}_2(\mathbf{n}) \quad , \quad \epsilon_2^{\mathcal{B}} = \max_{\mathbb{S}^2} \tilde{\epsilon}_1(\mathbf{n}) \quad , \quad (\text{II.1})$$

Globally, in the generic case, we have the relation

$$\max_{\mathbb{S}^2} \tilde{\epsilon}_1(\mathbf{n}) > \min_{\mathbb{S}^2} \tilde{\epsilon}_2(\mathbf{n})$$

Finding the functions $\tilde{\epsilon}_1(\mathbf{n})$ and $\tilde{\epsilon}_2(\mathbf{n})$ is in general a rather complex computational problem. However, for an approximate calculation of the width of the interval

$[\epsilon_1^{\mathcal{B}}, \epsilon_2^{\mathcal{B}}]$, one can use special methods that give a good (and in some cases accurate) estimate of its position. Here we use the method proposed in [44] and suitable for many relations $\epsilon(\mathbf{p})$ that have a fairly rich symmetry.

Namely, we first replace the expressions (II.1) with the expressions

$$\epsilon_1^{\mathcal{B}} = \min_{\cup \partial W_\alpha} \tilde{\epsilon}_0(\mathbf{n}) \quad , \quad \epsilon_2^{\mathcal{B}} = \max_{\cup \partial W_\alpha} \tilde{\epsilon}_0(\mathbf{n}) \quad (\text{II.2})$$

(the minimum and maximum are taken only along the boundaries of the Zones W_α), which give the same values of $\epsilon_1^{\mathcal{B}}$ and $\epsilon_2^{\mathcal{B}}$ for the majority of “physically realistic” relationships $\epsilon(\mathbf{p})$

Second, to evaluate the expressions (II.2), we use the values of $\tilde{\epsilon}_0(\mathbf{n})$ at the boundaries of the largest Zones W_α , where their variation is sufficiently large. More precisely, to evaluate the values of $\epsilon_1^{\mathcal{B}}$ and $\epsilon_2^{\mathcal{B}}$, we use the values of $\tilde{\epsilon}_0(P)$ and $\tilde{\epsilon}_0(Q)$ at the “symmetric” points P and Q of the boundary of the symmetric Zone W_1 , shown in Fig. 8, b. By tracking the disappearance of cylinders of closed trajectories on the corresponding

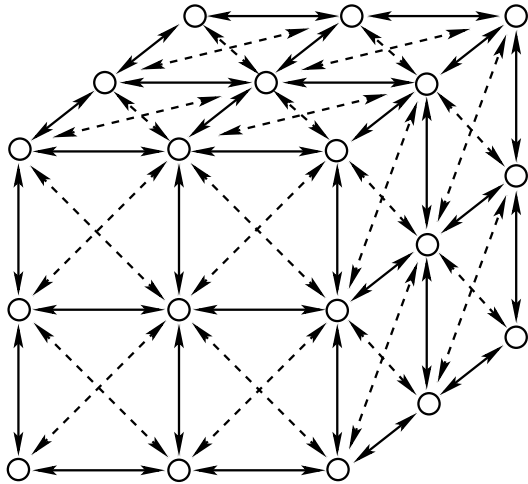


FIG. 10: Principal and additional jumps between nodes of a simple cubic lattice in the tight-binding approximation.

Fermi surfaces, we can determine the position of the points P and Q , as well as the values of $\tilde{\epsilon}_0(P)$ and $\tilde{\epsilon}_0(Q)$.

In this section, we estimate the position of the interval $[\epsilon_1^{\mathcal{B}}, \epsilon_2^{\mathcal{B}}]$ in the tight-binding approximation for a simple cubic lattice. For simplicity, we will use “dimensionless” values of ϵ and \mathbf{p} and denote the components \mathbf{p} by the usual coordinates $\mathbf{p} = (x, y, z)$.

As a correction to the leading approximation, we consider here jumps to sites next to the nearest ones (Fig. 10). The full dispersion relation takes then the form

$$\begin{aligned} \epsilon_{\delta}(\mathbf{p}) &= \cos x + \cos y + \cos z + \\ &+ \delta \left(\cos(x+y) + \cos(x-y) + \cos(x+z) + \right. \\ &\left. + \cos(x-z) + \cos(y+z) + \cos(y-z) \right) = \\ &= \cos x + \cos y + \cos z + \\ &+ 2\delta(\cos x \cos y + \cos x \cos z + \cos y \cos z) \quad (\text{II.3}) \end{aligned}$$

The equations of the Fermi surfaces

$$\begin{aligned} \cos x + \cos y + \cos z + \\ + 2\delta(\cos x \cos y + \cos x \cos z + \cos y \cos z) = \epsilon_F \end{aligned}$$

are invariant under the transformation

$$x \rightarrow x + \pi, \quad y \rightarrow y + \pi, \quad z \rightarrow z + \pi$$

$$\delta \rightarrow -\delta, \quad \epsilon_F \rightarrow -\epsilon_F$$

It can be seen, therefore, that the Fermi surfaces $\epsilon_{-\delta}(\mathbf{p}) = \epsilon_F$ are obtained from the surfaces $\epsilon_{\delta}(\mathbf{p}) = -\epsilon_F$ by a shift in \mathbf{p} -space. Thus, in the study of the trajectories of (I.1), it is sufficient for us to restrict ourselves to the values $\delta \geq 0$ (the reality of δ is a consequence of the symmetry of the lattice).

For $\delta = 0$ the Fermi surface $\epsilon(\mathbf{p}) = 0$ has genus 3 and rank 3 (Fig. 11) and this property is preserved for sufficiently small values of δ and ϵ_F .

For directions \mathbf{B} close to z , it is easy to distinguish cylinders C_1 and C_2 (of electron and hole type) that cut these surfaces into carriers of open trajectories for $\mathbf{n} \in W_1$ (and $\epsilon_F \in [\tilde{\epsilon}_1(\mathbf{n}), \tilde{\epsilon}_2(\mathbf{n})]$) (Fig. 11).

It is easy to see that the relation (II.3), as well as the Fermi surfaces $\epsilon(\mathbf{p}) = \epsilon_F$, are symmetric with respect to the planes

$$\Pi_n : x = \pi n, \quad n \in \mathbb{Z}$$

(as well as the planes $y = \pi n, z = \pi n, n \in \mathbb{Z}$).

The point $P \in \mathbb{S}^2$ (Fig. 8, b) corresponds to the disappearance of both cylinders C_1 and C_2 . According to Fig. 9, b, this corresponds to the emergence of cylinders of zero height containing a pair of saddle singular points of system (I.1). As is not difficult to see, by virtue of symmetry, these saddle singular points lie in the planes Π_n .

In the planes Π_n , the disappearance of the cylinders C_1 and C_2 corresponds to the simultaneous tangency of a pair of ovals defined by the relation

$$\epsilon(\mathbf{p}) \Big|_{\Pi_n} = \epsilon_F,$$

by some planes $\Pi(\mathbf{B})$, orthogonal to \mathbf{B} (or, equivalently, by lines $\Pi(\mathbf{B}) \cap \Pi_n$). In particular, in even planes Π_n , the lines $\Pi(\mathbf{B}) \cap \Pi_n$ must touch the pairs of ovals defined by the relation

$$\begin{aligned} \epsilon(\mathbf{p}) \Big|_{\Pi_n} &= \\ &= (1 + 2\delta)(\cos y + \cos z) + 2\delta \cos y \cos z = \epsilon_F - 1, \end{aligned}$$

and in odd ones

$$(1 - 2\delta)(\cos y + \cos z) + 2\delta \cos y \cos z = \epsilon_F + 1$$

(Fig. 12).

The equality of the slope of the tangents in the even and odd planes Π_n gives us the required dependence of ϵ_F (i.e. $\tilde{\epsilon}_0(P)$) on the value δ .

Similarly, the point $Q \in \mathbb{S}^2$ corresponds to the emergence of zero-height cylinders (C_1 and C_2) containing singular points of the system (I.1). As can be seen from the geometry of our Fermi surfaces, each zero-height cylinder now contains 4 saddle singular points of (I.1). For topological reasons, the total number of saddle singular points on our surfaces is also equal to 4. It follows then that each plane $\Pi(\mathbf{B})$ containing zero-height cylinders C_1 must also contain zero-height cylinders C_2 (adjacent to the same saddles).

For the value $\delta = 0$ we have $\tilde{\epsilon}_0(Q) = 0$, and the plane we need (for example) is the plane

$$z = (y - x)/2 \quad (\text{II.4})$$

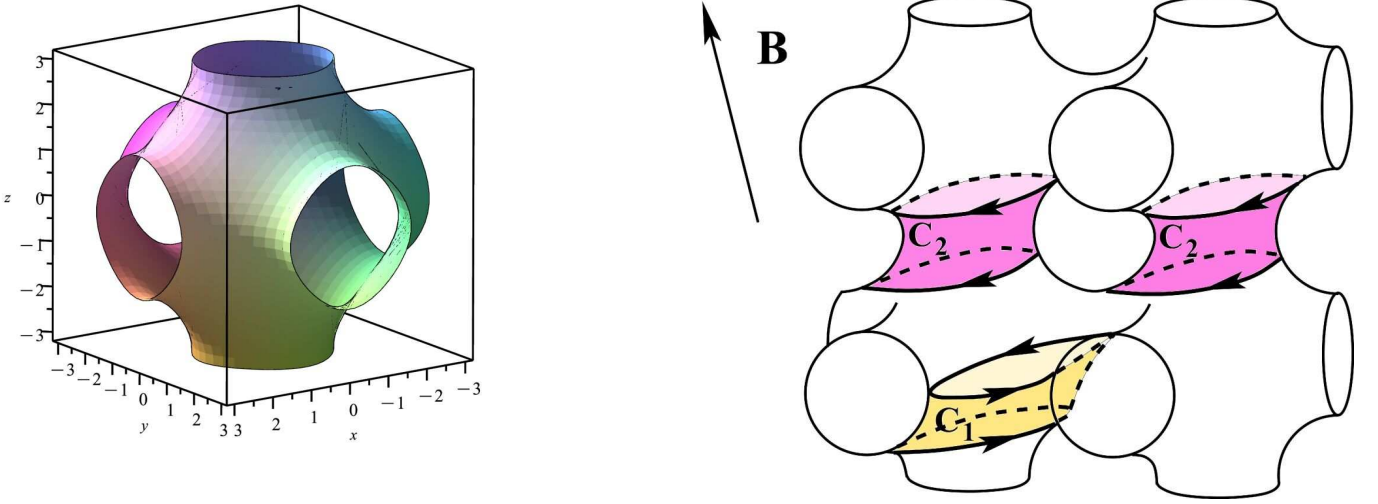


FIG. 11: The Fermi surfaces $\epsilon_F(\mathbf{p}) = \epsilon_F$ for sufficiently small values of δ and ϵ_F and cylinders of closed trajectories cutting the Fermi surfaces into carriers of open trajectories (simple cubic lattice).

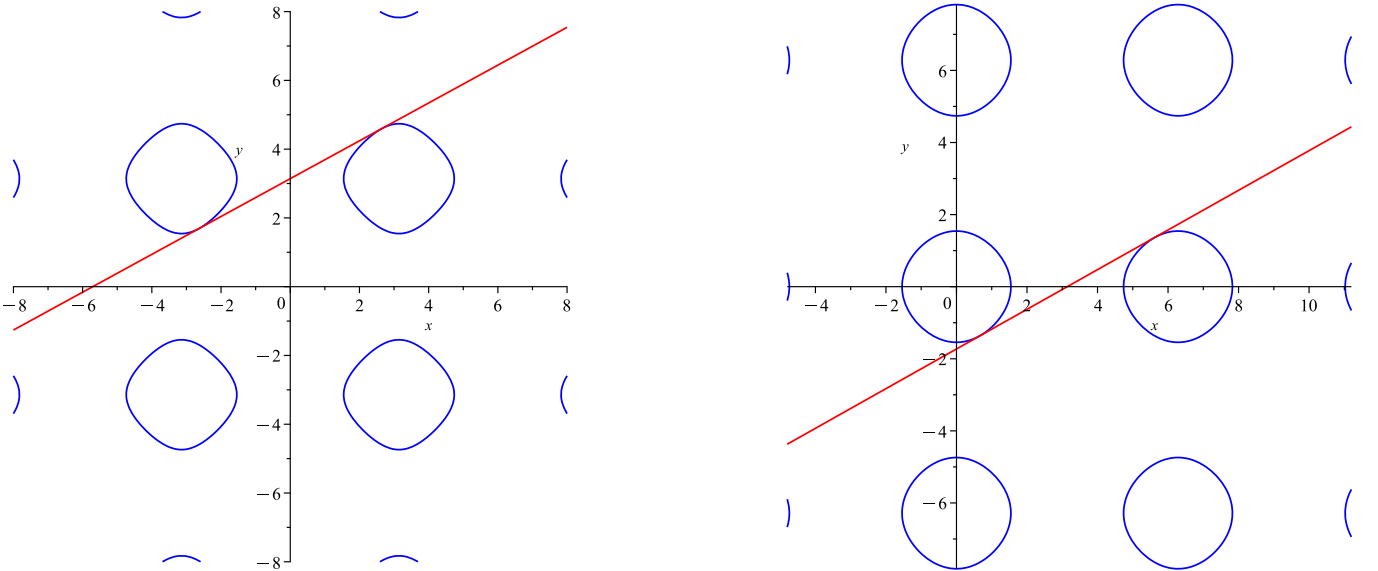


FIG. 12: Simultaneous tangency of a pair of ovals defined by the relation $\epsilon_\delta(\mathbf{p}) = \epsilon_F$ ($\delta = 0.2$, $\epsilon_F = -0.1728265816$) by straight lines $\Pi(\mathbf{B}) \cap \Pi_n$ in even and odd planes Π_n (simple cubic lattice).

As follows from the symmetry of the dispersion law (II.3), for $\delta \neq 0$, the plane $\Pi(\mathbf{B})$, containing zero-height electron-type cylinders, passes through the points $(-\pi, -\pi, 0)$ and $(\pi, \pi, 0)$ (the centers of the cylinders). Similarly, the plane $\Pi(\mathbf{B})$, containing zero-height hole-type cylinders, passes through the points $(0, -2\pi, \pi)$ and $(2\pi, 0, \pi)$. Both of these planes obviously coincide with the plane (II.4) for $\delta = 0$. In view of the above, however, these planes must coincide with each other also for $\delta \neq 0$. This means that the plane (II.4) remains unchanged for $\delta \neq 0$, and only the value of $\tilde{\epsilon}_0(Q, \delta)$, as well as the position of the singular points inside this plane, change

(Fig. 13). In other words, in our case, the position of the point $Q \in \mathbb{S}^2$ remains unchanged under variations of δ .

Due to the symmetry of the problem, to find the value $\tilde{\epsilon}_0(Q, \delta)$ it is sufficient to impose the condition of tangency of the plane (II.4) and the surface $\epsilon_\delta(\mathbf{p}) = \tilde{\epsilon}_0(Q, \delta)$ at one of the saddle points (with coordinates (x, y, z)). The tangency condition implies collinearity of the gradi-

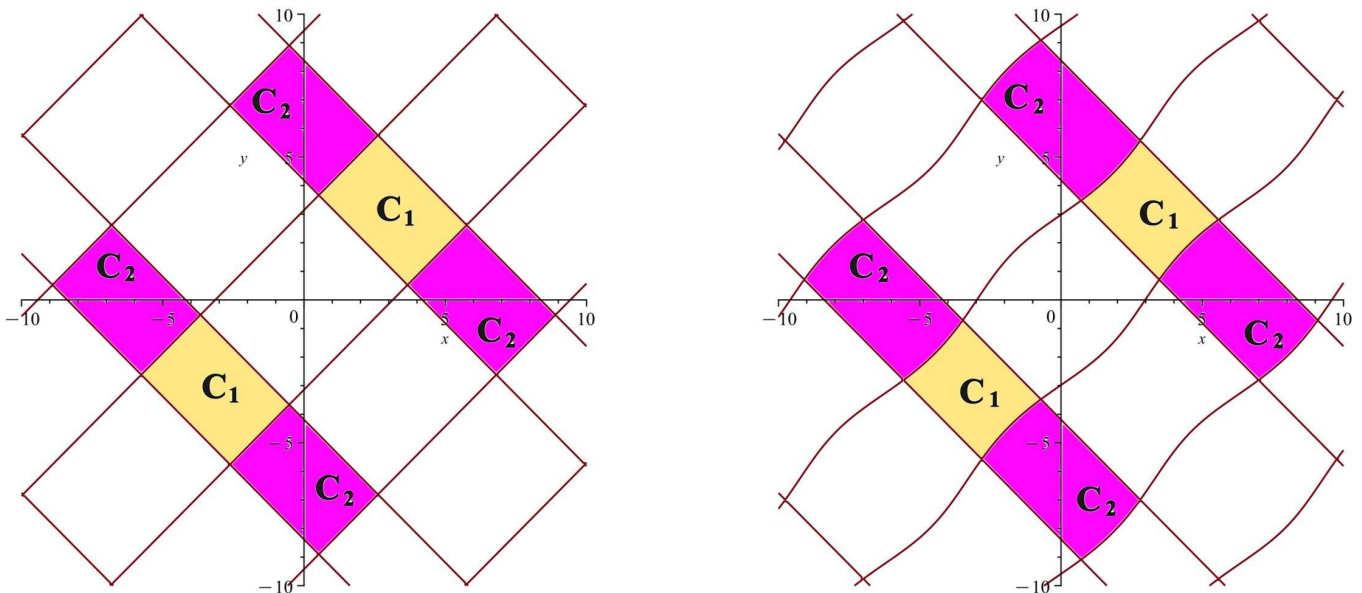


FIG. 13: The level lines $\epsilon_0(\mathbf{p}) = 0$ and $\epsilon_\delta(\mathbf{p}) = \epsilon_F$ ($\delta = 0.2$, $\epsilon_F = -0.3$) in the plane (II.4) for the dispersion law (II.3) (simple cubic lattice).

ent of $\epsilon_\delta(\mathbf{p})$

$$\begin{aligned} \nabla \epsilon_\delta(\mathbf{p}) &= \begin{pmatrix} -\sin x (1 + 2\delta \cos y + 2\delta \cos z) \\ -\sin y (1 + 2\delta \cos x + 2\delta \cos z) \\ -\sin z (1 + 2\delta \cos x + 2\delta \cos y) \end{pmatrix} = \\ &= \begin{pmatrix} -\sin x \left(1 + 2\delta \cos y + 2\delta \cos \frac{y-x}{2}\right) \\ -\sin y \left(1 + 2\delta \cos x + 2\delta \cos \frac{y-x}{2}\right) \\ -\sin \frac{y-x}{2} (1 + 2\delta \cos x + 2\delta \cos y) \end{pmatrix} \end{aligned}$$

and the vector $(1, -1, 2)$ at the point (x, y, z) .

Solving the system

$$\begin{aligned} \cos x + \cos y + \cos \frac{y-x}{2} + \\ + 2\delta \left(\cos x \cos y + (\cos x + \cos y) \cos \frac{y-x}{2} \right) &= \\ &= \tilde{\epsilon}_0(Q, \delta) \end{aligned}$$

$$\begin{aligned} \sin x \left(1 + 2\delta \cos y + 2\delta \cos \frac{y-x}{2} \right) &= \\ = -\sin y \left(1 + 2\delta \cos x + 2\delta \cos \frac{y-x}{2} \right) \end{aligned}$$

$$\begin{aligned} \sin x \left(1 + 2\delta \cos y + 2\delta \cos \frac{y-x}{2} \right) &= \\ = \frac{1}{2} \sin \frac{y-x}{2} \left(1 + 2\delta \cos x + 2\delta \cos y \right) \end{aligned}$$

with respect to x , y and $\tilde{\epsilon}_0(Q, \delta)$, we obtain the dependence we need.

The values of the functions $\tilde{\epsilon}_0(P)$ and $\tilde{\epsilon}_0(Q)$ are presented in Fig. 14. Everywhere in the interval $0 < \delta < 0.5$ we have the relation $\tilde{\epsilon}_0(P) < \tilde{\epsilon}_0(Q)$ (and $\tilde{\epsilon}_0(P) > \tilde{\epsilon}_0(Q)$ in the interval $-0.5 < \delta < 0$). As is easy to see, near the value $\delta = 0.5$ the width of the interval

$$[\epsilon_1^B, \epsilon_2^B] \simeq [\tilde{\epsilon}_0(P), \tilde{\epsilon}_0(Q)]$$

is of the order of 1.5% of the conduction band width.

For $\delta \simeq 0.5$, the topology of the Fermi surfaces near the interval $[\tilde{\epsilon}_0(P), \tilde{\epsilon}_0(Q)]$ changes. Specifically, the Fermi surfaces acquire additional (very thin) ‘‘handles’’ and their genus increases to 7. For $\delta > 0.5$, therefore, the interval $[\tilde{\epsilon}_0(P), \tilde{\epsilon}_0(Q)]$ must be estimated based on the new geometry of the Fermi surfaces. In this paper, we consider the higher terms in (II.3) as corrections to the main approximation, so we restrict ourselves here to the range of values $-0.5 < \delta < 0.5$ for the simple cubic lattice.

III. BODY-CENTERED CUBIC LATTICE

As in the previous section, we will consider here the approximation based on jumps between the nearest and next lattice nodes (Fig. 15). In the ‘‘dimensionless’’ quantities ϵ and \mathbf{p} , it will be convenient to use the following

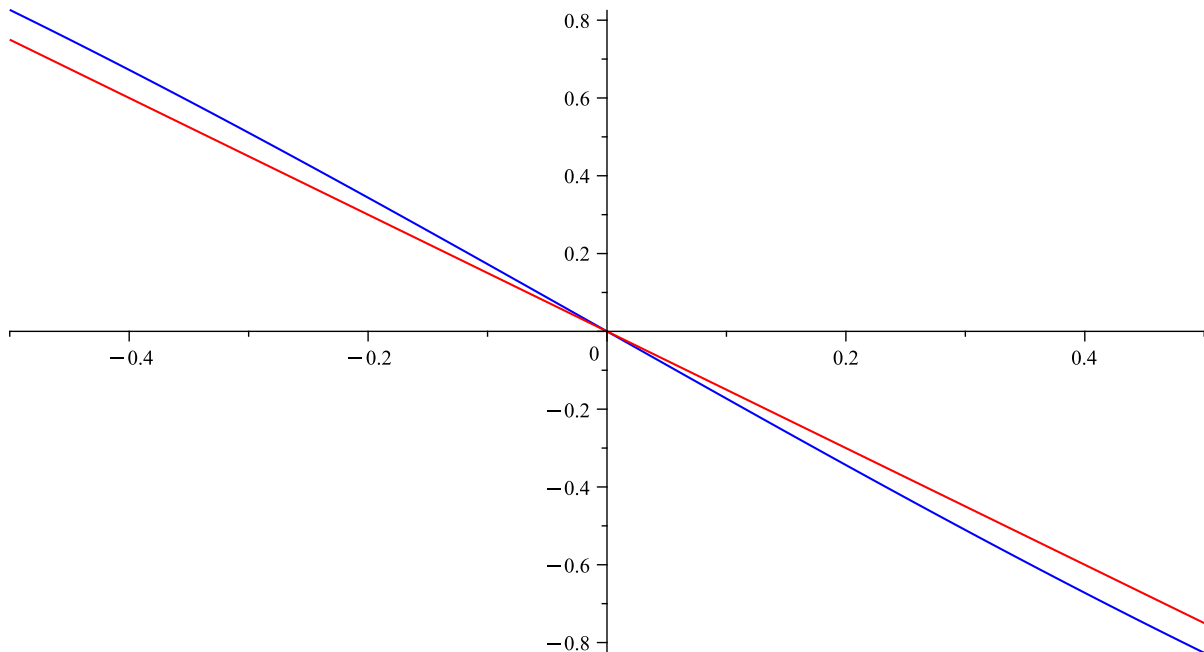


FIG. 14: The values $\tilde{\epsilon}_0(P, \delta)$ and $\tilde{\epsilon}_0(Q, \delta)$ for the dispersion law (II.3) in the interval $-0.5 < \delta < 0.5$ (simple cubic lattice).

normalization

$$\begin{aligned} \epsilon(\mathbf{p}) &= \frac{1}{4} \left[\cos(x+y+z) + \cos(x+y-z) + \right. \\ &\quad \left. + \cos(x-y+z) + \cos(-x+y+z) + \right. \\ &\quad \left. + \delta \cos 2x + \delta \cos 2y + \delta \cos 2z \right] = \\ &= \cos x \cdot \cos y \cdot \cos z + \frac{\delta}{4} (\cos 2x + \cos 2y + \cos 2z) \end{aligned} \quad (\text{III.1})$$

Here it is also easy to see that the shift

$$x \rightarrow x + \pi, \quad y \rightarrow y + \pi, \quad z \rightarrow z + \pi$$

transforms the surfaces $\epsilon_{-\delta}(\mathbf{p}) = \epsilon_F$ into the surfaces $\epsilon_{\delta}(\mathbf{p}) = -\epsilon_F$. Thus, as before, it is sufficient for us to study here the case $\delta \geq 0$ and use the same picture of trajectories for $\delta \leq 0$ with the replacement $\epsilon_F \rightarrow -\epsilon_F$.

The zeroth-order dispersion relation

$$\epsilon(\mathbf{p}) = \cos x \cdot \cos y \cdot \cos z$$

has here special properties. Namely, an extended Fermi surface arises here only for the value $\epsilon_F = 0$, for all $\epsilon_F < 0$ and $\epsilon_F > 0$ the Fermi surfaces

$$\cos x \cdot \cos y \cdot \cos z = \epsilon_F \quad (\text{III.2})$$

are compact (Fig. 16).

It is easy to see that both for $\epsilon_F < 0$ and for $\epsilon_F > 0$ all trajectories of (I.1) are closed for all directions of \mathbf{B}

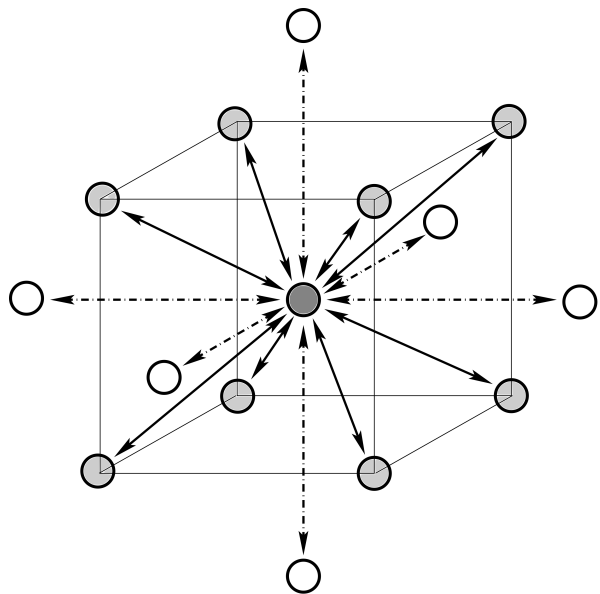


FIG. 15: Main and additional jumps in the body-centered cubic lattice.

(and are of electron and hole type, respectively). As a consequence, we have here in the zeroth approximation

$$\epsilon_1^A = \epsilon_1^B = \epsilon_2^B = \epsilon_2^A = 0$$

Thus, the emergence of the second term in (III.1) leads here not only to a non-zero width of the interval $[\epsilon_1^B, \epsilon_2^B]$, but also of the interval $(\epsilon_1^A, \epsilon_2^A)$.

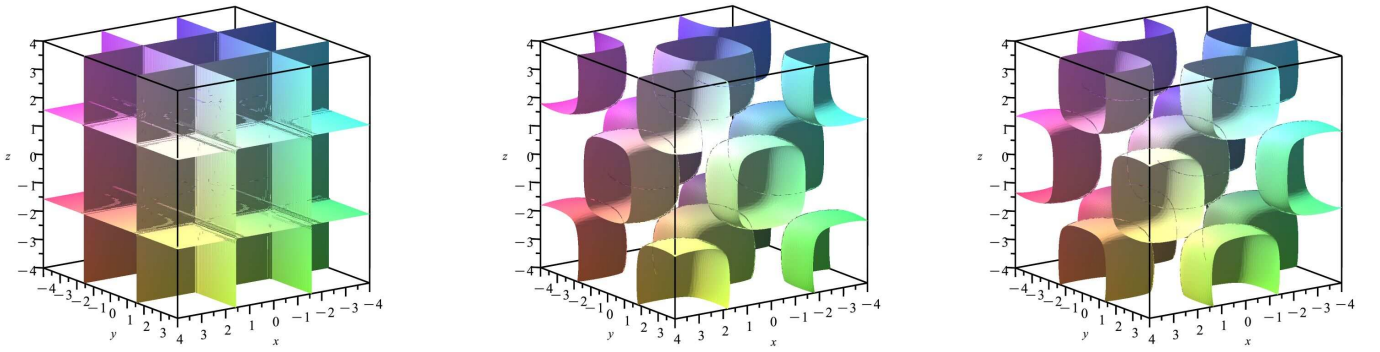


FIG. 16: The Fermi surfaces (III.2) for $\epsilon_F = 0$, $\epsilon_F < 0$ and $\epsilon_F > 0$.

For $\delta > 0$ the dispersion relation (III.1) becomes a generic relation. As is not difficult to show, extended Fermi surfaces arise here in the interval

$$\epsilon_F \in (\epsilon_1^A, \epsilon_2^A) = \left(-\frac{3\delta}{4} + \frac{\delta^3}{2}, -\frac{\delta}{4} \right)$$

(and symmetrically for $\delta < 0$).

In the intervals $\epsilon_F \in (\epsilon_1^A, \epsilon_2^A)$ the Fermi surfaces have genus 6 (and rank 3) (Fig. 17).

Here we use the intervals $[\tilde{\epsilon}_0(Q, \delta), \tilde{\epsilon}_0(P, \delta)]$ (Fig. 8) to estimate the intervals $[\epsilon_1^B(\delta), \epsilon_2^B(\delta)]$. As we have already said, in the general case we have the inclusion

$$[\tilde{\epsilon}_0(Q, \delta), \tilde{\epsilon}_0(P, \delta)] \subseteq [\epsilon_1^B(\delta), \epsilon_2^B(\delta)] ,$$

moreover, for large Zones W_α these intervals coincide in order of magnitude (and often coincide exactly).

Near the intervals $[\tilde{\epsilon}_0(Q, \delta), \tilde{\epsilon}_0(P, \delta)]$, the geometry of the Fermi surfaces for the relation (III.1) can be described relatively simply. Namely, the Fermi surfaces here are formed by “spheroids” located at the nodes of a face-centered lattice (note that the lattice inverse to the body-centered lattice is face-centered), connected by (very short) cylinders. It should be noted that the cross-sections of these cylinders have different shapes for different values of δ (Fig. 18).

For directions of \mathbf{B} close to \hat{z} , Fermi surfaces contain 4 carriers of open trajectories $\{T_1, T_2, T_3, T_4\}$, separated by 5 cylinders of closed trajectories $\{C_1^-, C_2^-, C_3^-, C_1^+, C_2^+\}$ (Fig. 19).

Obviously, the cylinder C_1^- is symmetric with respect to the reflection $\mathbf{p} \rightarrow -\mathbf{p}$, while the cylinders C_2^-, C_3^- , as well as C_1^+, C_2^+ , transform into each other under this reflection. The topological diagram of the connection of the carriers T_1, T_2, T_3, T_4 and the cylinders $C_1^-, C_2^-, C_3^-, C_1^+, C_2^+$ is shown in Fig. 20.

The disappearance of any of the cylinders upon deviation of $\mathbf{n} = \mathbf{B}/B$ from \hat{z} leads to the destruction of the carriers of open trajectories connected by it (the possibility of trajectories jumping from one carrier to another appears). This destruction, however, can be eliminated

by changing the value of ϵ_F , if it is not accompanied at the same time by the disappearance of another cylinder of closed trajectories of the opposite type. As we have already mentioned, the boundaries of the Zones W_α are therefore determined by the disappearance of at least one cylinder of the electron type and one of the hole type (and the destruction of all carriers of open trajectories).

Due to symmetry, both hole-type cylinders (C_1^+ and C_2^+) disappear simultaneously (for the same \mathbf{B} directions). As a consequence, any point on the boundary W_1 corresponds to the simultaneous disappearance of the cylinders C_1^+ and C_2^+ .

In our case, for the impossibility of restoring any of the pairs of carriers of open trajectories ($\{T_1, T_2\}$ or $\{T_3, T_4\}$) under a change of the value of ϵ_F , the absence of all the cylinders C_1^-, C_2^-, C_3^- is required (Fig. 20).

Thus, the boundary of W_1 is determined by the disappearance of the pair $\{C_1^+, C_2^+\}$, and also either the cylinder C_1^- , or the pair $\{C_2^-, C_3^-\}$ (depending on which disappears last).

From the shape of the Fermi surfaces for different δ (Fig. 18), one can see that the height of the cylinder C_1^- is quite large, and the heights of the cylinders C_2^- and C_3^- are quite small, for small values of δ . For $\delta \rightarrow 1$ the situation is reversed, i.e. the height of C_1^- becomes small, and the heights of C_2^- and C_3^- increase noticeably. It can be stated, therefore, that for small values of δ the position of points P and Q is determined by the disappearance of the cylinders $\{C_1^+, C_2^+, C_1^-\}$, and for $\delta \rightarrow 1$ - by the disappearance of the cylinders $\{C_1^+, C_2^+, C_2^-, C_3^-\}$.

Fig. 21, a, shows the section of the Fermi surfaces $\epsilon_\delta(\mathbf{p}) = \tilde{\epsilon}_0(P)$ by special planes $\Pi_{1,2}(\mathbf{B}) \perp \mathbf{B}$ for the point P determined by the disappearance of the cylinders C_1^-, C_1^+ and C_2^+ .

The plane $\Pi_1(\mathbf{B})$ is defined by the equation $z = \mu y$ (with some coefficient μ) and is tangent to S_F , in particular, at points A and B with some coordinates $(b, a, \mu a)$ and $(b, -a, -\mu a)$.

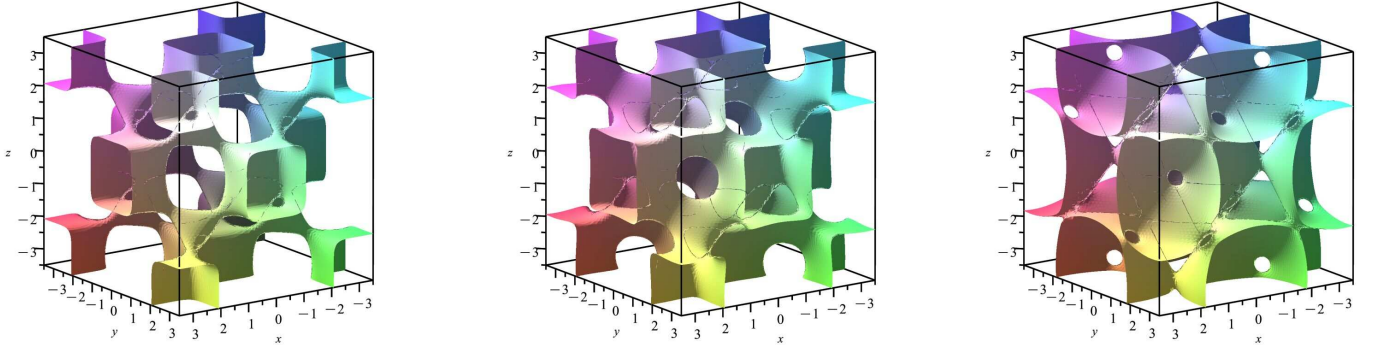


FIG. 17: The Fermi surfaces $\epsilon_\delta(\mathbf{p}) = \epsilon_F$ for $\epsilon_F = -0.3$, $\epsilon_F = -0.22$ and $\epsilon_F = -0.14$ ($\delta = 0.5$) for the relation (III.1)

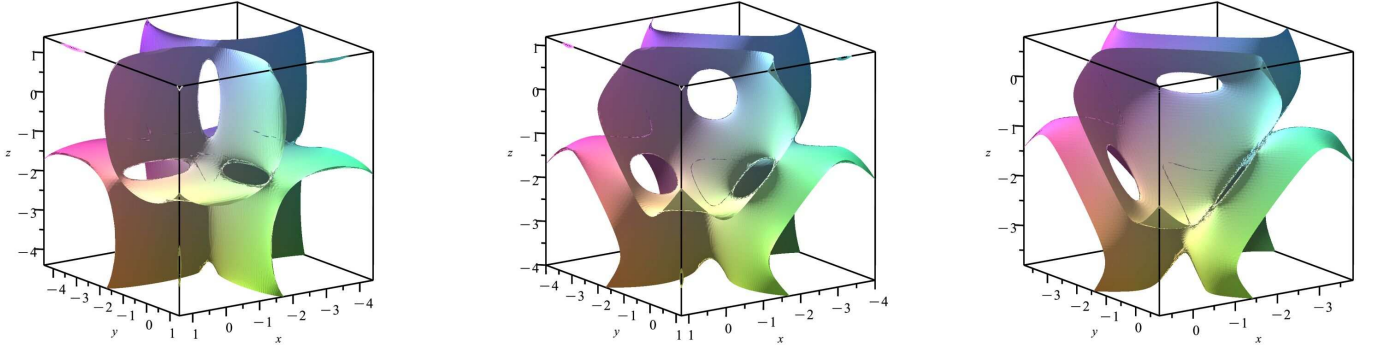


FIG. 18: The Fermi surfaces $\epsilon_{0.1}(\mathbf{p}) = -0.06$, $\epsilon_{0.5}(\mathbf{p}) = -0.2$, $\epsilon_{0.9}(\mathbf{p}) = -0.245$ for the relation (III.1) (body-centered lattice).

The plane $\Pi_2(\mathbf{B})$ is given by the equation

$$(z - 2\mu a) = \mu y$$

and touches S_F at a point C with coordinates $(0, c, \mu c + 2\mu a)$.

We have, therefore,

$$\epsilon_\delta(b, a, \mu a) = \tilde{\epsilon}_0(P, \delta)$$

$$\epsilon_\delta(0, c, \mu c + 2\mu a) = \tilde{\epsilon}_0(P, \delta)$$

$$\nabla \epsilon_\delta(b, a, \mu a) \parallel (0, -\mu, 1)$$

$$\nabla \epsilon_\delta(0, c, \mu c + 2\mu a) \parallel (0, -\mu, 1)$$

(touching at the point B occurs automatically), or

$$\begin{aligned} \cos b \cos a \cos \mu a + \\ + \frac{\delta}{4} (\cos 2b + \cos 2a + \cos 2\mu a) = \tilde{\epsilon}_0(P, \delta), \end{aligned}$$

$$\begin{aligned} \cos c \cos(\mu c + 2\mu a) + \\ + \frac{\delta}{4} (1 + \cos 2c + \cos(2\mu c + 4\mu a)) = \tilde{\epsilon}_0(P, \delta), \end{aligned}$$

$$\cos a \cos \mu a + \delta \cos b = 0,$$

$$\begin{aligned} \cos b \sin a \cos \mu a + \delta \sin a \cos a + \\ + \mu \cos b \cos a \sin \mu a + \mu \delta \sin \mu a \cos \mu a = 0, \end{aligned}$$

$$\begin{aligned} \mu \cos c \sin(\mu c + 2\mu a) + \mu \delta \sin(\mu c + 2\mu a) \cos(\mu c + 2\mu a) + \\ + \sin c \cos(\mu c + 2\mu a) + \delta \sin c \cos c = 0 \quad (\text{III.3}) \end{aligned}$$

Fig. 21, b, shows the section of the Fermi surfaces $\epsilon_\delta(\mathbf{p}) = \tilde{\epsilon}_0(P)$ by special planes $\Pi_{1,2}(\mathbf{B}) \perp \mathbf{B}$ for the point P determined by the disappearance of the cylinders C_2^- , C_3^- , C_1^+ and C_2^+ .

The plane $\Pi_1(\mathbf{B})$ is now given by the equation

$$z - \frac{\pi}{2} = \mu \left(y - \frac{\pi}{2} \right)$$

(with some coefficient μ) and is tangent to S_F at a point A with some coordinates $(b, a, \mu a + \pi(1 - \mu)/2)$.

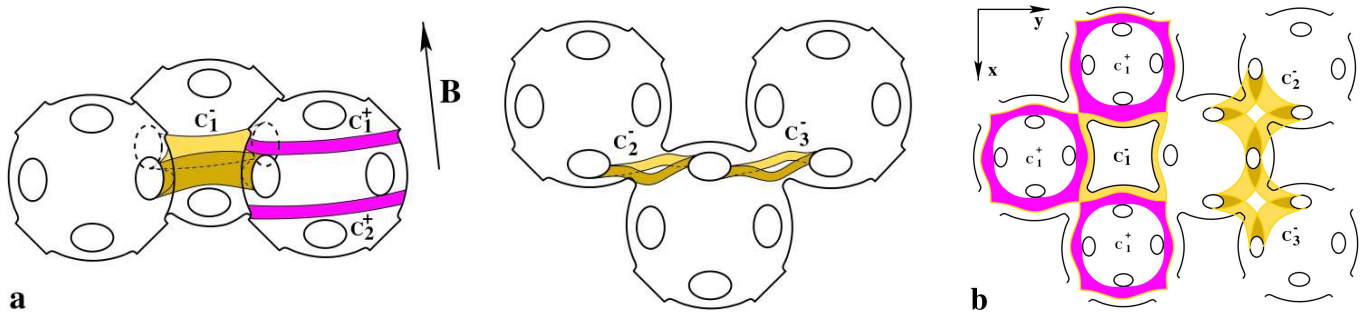


FIG. 19: (a) Cylinders $C_1^-, C_1^+, C_2^+, C_2^-, C_3^-$ for a direction \mathbf{B} , close to \hat{z} . (b) Shape of the cylinders C_1^-, C_2^- and C_3^- for $\mathbf{B} \parallel \hat{z}$ (top view).

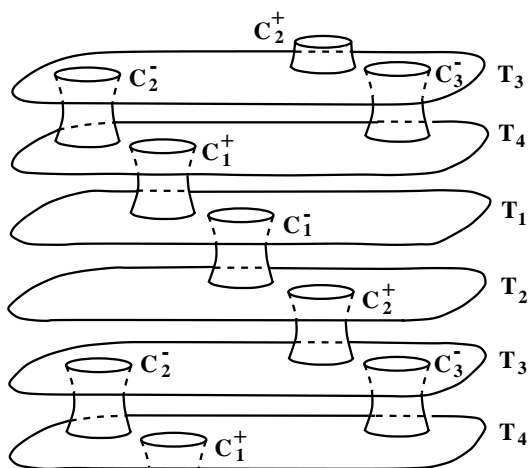


FIG. 20: Topological diagram of the connection of carriers T_1, T_2, T_3, T_4 and cylinders $C_1^-, C_2^-, C_3^-, C_1^+, C_2^+$ into the Fermi surface at $\mathbf{n} \simeq \hat{z}$ (body-centered lattice).

The plane $\Pi_2(\mathbf{B})$ is given by the equation

$$z = \mu y + \lambda$$

(with some λ) and touches S_F at point C with coordinates $(0, c, \mu c + \lambda)$ and point B with coordinates $(h, d, \mu d + \lambda)$.

We have now

$$\epsilon_\delta(b, a, \mu a + \pi(1 - \mu)/2) = \tilde{\epsilon}_0(P, \delta)$$

$$\epsilon_\delta(0, c, \mu c + \lambda) = \tilde{\epsilon}_0(P, \delta)$$

$$\epsilon_\delta(h, d, \mu d + \lambda) = \tilde{\epsilon}_0(P, \delta)$$

$$\nabla \epsilon_\delta(b, a, \mu a + \pi(1 - \mu)/2) \parallel (0, -\mu, 1)$$

$$\nabla \epsilon_\delta(0, c, \mu c + \lambda) \parallel (0, -\mu, 1)$$

$$\nabla \epsilon_\delta(h, d, \mu d + \lambda) \parallel (0, -\mu, 1)$$

or

$$\frac{\delta}{4} \left(\cos 2b + \cos 2a + \cos 2(\mu a + \pi(1 - \mu)/2) \right) + \cos b \cos a \cos(\mu a + \pi(1 - \mu)/2) = \tilde{\epsilon}_0(P, \delta),$$

$$\frac{\delta}{4} \left(1 + \cos 2c + \cos 2(\mu c + \lambda) \right) + \cos c \cos(\mu c + \lambda) = \tilde{\epsilon}_0(P, \delta),$$

$$\frac{\delta}{4} \left(\cos 2h + \cos 2d + \cos 2(\mu d + \lambda) \right) + \cos h \cos d \cos(\mu d + \lambda) = \tilde{\epsilon}_0(P, \delta),$$

$$\cos a \cos(\mu a + \pi(1 - \mu)/2) + \delta \cos b = 0,$$

$$\cos b \sin a \cos(\mu a + \pi(1 - \mu)/2) + \delta \sin a \cos a + \mu \left(\cos b \cos a + \delta \cos(\mu a + \pi(1 - \mu)/2) \right) \times \sin(\mu a + \pi(1 - \mu)/2) = 0,$$

$$\mu \cos c \sin(\mu c + \lambda) + \mu \delta \sin(\mu c + \lambda) \cos(\mu c + \lambda) + \sin c \cos(\mu c + \lambda) + \delta \sin c \cos c = 0,$$

$$\cos d \cos(\mu d + \lambda) + \delta \cos h = 0,$$

$$\cos h \sin d \cos(\mu d + \lambda) + \delta \sin d \cos d + \mu \left(\cos h \cos d + \delta \cos(\mu d + \lambda) \right) \sin(\mu d + \lambda) = 0 \quad (\text{III.4})$$

By independently solving systems (III.3) and (III.4) and choosing for each δ the solution corresponding to

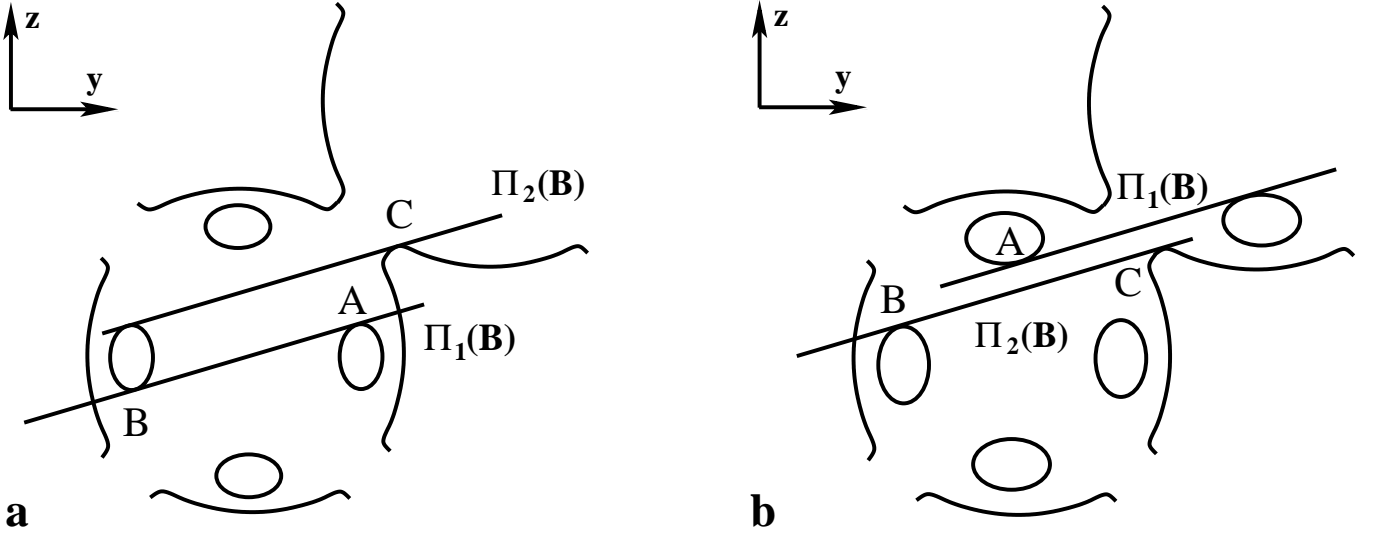


FIG. 21: (a) Section of the Fermi surface $\epsilon_\delta(\mathbf{p}) = \tilde{\epsilon}_0(P)$ by planes $\Pi_{1,2}(\mathbf{B})$ containing cylinders C_1^- and C_1^+ , C_2^+ of zero height. (b) Section of the Fermi surface $\epsilon_\delta(\mathbf{p}) = \tilde{\epsilon}_0(P)$ by planes $\Pi_{1,2}(\mathbf{B})$ containing cylinders C_2^- , C_3^- and C_1^+ , C_2^+ of zero height (projection onto the yz -plane).

the larger value of μ , we obtain the dependence $\tilde{\epsilon}_0(P)$ that we need.

For the direction $\mathbf{n} = Q$ it is convenient to make the substitution

$$x = \frac{v-u}{\sqrt{2}}, \quad y = \frac{v+u}{\sqrt{2}}$$

As is easy to verify, in the new coordinates the dispersion relation (III.1) has the form

$$\begin{aligned} \epsilon_\delta(\mathbf{p}) = & \frac{1}{2} \left(\cos \sqrt{2}u + \cos \sqrt{2}v \right) \cos z + \\ & + \frac{\delta}{2} \cos \sqrt{2}u \cdot \cos \sqrt{2}v + \frac{\delta}{4} \cos 2z \end{aligned}$$

Fig. 22, a, shows the section of the Fermi surfaces $\epsilon_\delta(\mathbf{p}) = \tilde{\epsilon}_0(Q)$ by special planes $\Pi_{1,2}(\mathbf{B}) \perp \mathbf{B}$ for the point Q determined by the disappearance of the cylinders C_1^- , C_1^+ and C_2^+ .

The plane $\Pi_1(\mathbf{B})$ is given in new coordinates by the equation

$$z = \nu \left(u - \frac{\pi}{\sqrt{2}} \right)$$

(with some ν) and touches S_F at point C with coordinates $(c, \pi/\sqrt{2}, \nu(c - \pi/\sqrt{2}))$.

The plane $\Pi_2(\mathbf{B})$ is given by the equation

$$z = \nu u + \zeta$$

(with some ζ) and touches S_F at point A with coordinates $(a, 0, \nu a + \zeta)$ and at point B with coordinates $(b, h, \nu b + \zeta)$.

The complete system for the problem parameters has the form

$$\begin{aligned} & \frac{1}{2} \left(\cos \sqrt{2}c - 1 \right) \cos \nu(c - \pi/\sqrt{2}) - \\ & - \frac{\delta}{2} \cos \sqrt{2}c + \frac{\delta}{4} \cos 2\nu(c - \pi/\sqrt{2}) = \tilde{\epsilon}_0(Q, \delta), \end{aligned}$$

$$\begin{aligned} & \frac{1}{2} \left(\cos \sqrt{2}a + 1 \right) \cos(\nu a + \zeta) + \\ & + \frac{\delta}{2} \cos \sqrt{2}a + \frac{\delta}{4} \cos 2(\nu a + \zeta) = \tilde{\epsilon}_0(Q, \delta), \end{aligned}$$

$$\begin{aligned} & \frac{1}{2} \left(\cos \sqrt{2}b + \cos \sqrt{2}h \right) \cos(\nu b + \zeta) + \\ & + \frac{\delta}{2} \cos \sqrt{2}b \cdot \cos \sqrt{2}h + \frac{\delta}{4} \cos 2(\nu b + \zeta) = \tilde{\epsilon}_0(Q, \delta), \end{aligned}$$

$$\begin{aligned} & \nu \left(\cos \sqrt{2}c - 1 \right) \sin \nu(c - \pi/\sqrt{2}) + \nu \delta \sin 2\nu(c - \pi/\sqrt{2}) + \\ & + \sqrt{2} \sin \sqrt{2}c \cos \nu(c - \pi/\sqrt{2}) - \sqrt{2} \delta \sin \sqrt{2}c = 0, \end{aligned}$$

$$\begin{aligned} & \nu \left(\cos \sqrt{2}a + 1 \right) \sin(\nu a + \zeta) + \nu \delta \sin 2(\nu a + \zeta) + \\ & + \sqrt{2} \sin \sqrt{2}a \cos(\nu a + \zeta) + \sqrt{2} \delta \sin \sqrt{2}a = 0, \end{aligned}$$

$$\cos(\nu b + \zeta) + \delta \cos \sqrt{2}b = 0,$$

$$\begin{aligned} & \nu \left(\cos \sqrt{2}b + \cos \sqrt{2}h \right) \sin(\nu b + \zeta) + \nu \delta \sin 2(\nu b + \zeta) + \\ & + \sqrt{2} \sin \sqrt{2}b \cos(\nu b + \zeta) + \sqrt{2} \delta \sin \sqrt{2}b \cos \sqrt{2}h = 0 \end{aligned} \quad (\text{III.5})$$

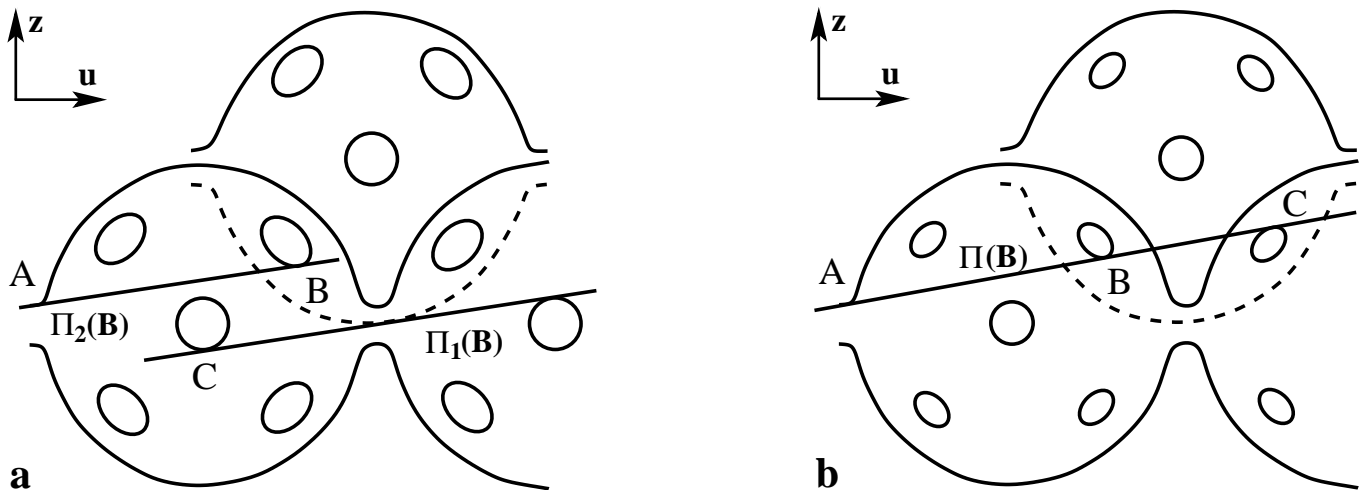


FIG. 22: (a) Section of the Fermi surface $\epsilon_\delta(\mathbf{p}) = \tilde{\epsilon}_0(Q)$ by the planes $\Pi_{1,2}(\mathbf{B})$ containing the cylinders C_1^- and C_1^+ , C_2^+ of zero height. (b) Section of the Fermi surface $\epsilon_\delta(\mathbf{p}) = \tilde{\epsilon}_0(Q)$ by the plane $\Pi(\mathbf{B})$ containing the cylinders C_2^- , C_3^- and C_1^+ , C_2^+ of zero height (projection onto the plane $x+y=0$).

Fig. 22, b, shows the section of the Fermi surfaces $\epsilon_\delta(\mathbf{p}) = \tilde{\epsilon}_0(Q)$ by a special plane $\Pi(\mathbf{B}) \perp \mathbf{B}$ for the point Q determined by the disappearance of the cylinders C_2^- , C_3^- , C_1^+ and C_2^+ .

The plane $\Pi(\mathbf{B})$ is given by the equation $z = \nu u + \lambda$ (with some ν and λ) and is tangent to the surface S_F at 5 (non-equivalent) points. By virtue of symmetry, to determine the dependence $\tilde{\epsilon}_0(Q)$ we only need to consider its tangency at 3 points A , B and C with coordinates $(a_1, 0, a_3)$, (b_1, b_2, b_3) , (c_1, c_2, c_3) (their projections are shown in Fig. 22).

The complete system for the problem parameters now has the form

$$\frac{1}{2} \left(\cos \sqrt{2}a_1 + 1 \right) \cos a_3 + \frac{\delta}{2} \cos \sqrt{2}a_1 + \frac{\delta}{4} \cos 2a_3 = \tilde{\epsilon}_0(Q, \delta),$$

$$\frac{1}{2} \left(\cos \sqrt{2}b_1 + \cos \sqrt{2}b_2 \right) \cos b_3 + \frac{\delta}{2} \cos \sqrt{2}b_1 \cdot \cos \sqrt{2}b_2 + \frac{\delta}{4} \cos 2b_3 = \tilde{\epsilon}_0(Q, \delta),$$

$$\frac{1}{2} \left(\cos \sqrt{2}c_1 + \cos \sqrt{2}c_2 \right) \cos c_3 + \frac{\delta}{2} \cos \sqrt{2}c_1 \cdot \cos \sqrt{2}c_2 + \frac{\delta}{4} \cos 2c_3 = \tilde{\epsilon}_0(Q, \delta),$$

$$\nu = \frac{b_3 - a_3}{b_1 - a_1} = \frac{c_3 - b_3}{c_1 - b_1},$$

$$\cos b_3 + \delta \cos \sqrt{2}b_1 = \cos c_3 + \delta \cos \sqrt{2}c_1 = 0,$$

$$\sqrt{2} \sin \sqrt{2}a_1 \cdot \cos a_3 + \sqrt{2}\delta \sin \sqrt{2}a_1 + \nu \sin a_3 \left(\cos \sqrt{2}a_1 + 1 \right) + \nu\delta \sin 2a_3 = 0,$$

$$\sqrt{2} \sin \sqrt{2}b_1 \cdot \cos b_3 + \sqrt{2}\delta \sin \sqrt{2}b_1 \cdot \cos \sqrt{2}b_2 + \nu \sin b_3 \left(\cos \sqrt{2}b_1 + \cos \sqrt{2}b_2 \right) + \nu\delta \sin 2b_3 = 0,$$

$$\sqrt{2} \sin \sqrt{2}c_1 \cdot \cos c_3 + \sqrt{2}\delta \sin \sqrt{2}c_1 \cdot \cos \sqrt{2}c_2 + \nu \sin c_3 \left(\cos \sqrt{2}c_1 + \cos \sqrt{2}c_2 \right) + \nu\delta \sin 2c_3 = 0 \quad (\text{III.6})$$

By independently solving systems (III.5) and (III.6) and choosing for each δ the solution corresponding to the larger value of ν , we obtain the dependence $\tilde{\epsilon}_0(Q)$ that we need.

Fig. 23 shows the values of the functions $\tilde{\epsilon}_0(P)$ and $\tilde{\epsilon}_0(Q)$, as well as the boundaries of the interval $(\epsilon_1^A(\delta), \epsilon_2^A(\delta))$ in the range $-1 < \delta < 1$. It can be seen that the width of the interval $[\tilde{\epsilon}_0(Q, \delta), \tilde{\epsilon}_0(P, \delta)]$ does not exceed here 0.1 of the width of the interval $(\epsilon_1^A(\delta), \epsilon_2^A(\delta))$. It can also be seen that the maximum width of the interval $[\tilde{\epsilon}_0(Q, \delta), \tilde{\epsilon}_0(P, \delta)]$ (for $\delta \simeq 0.6$) does not exceed 1% of the width of the interval $[\epsilon_{\min}(\delta), \epsilon_{\max}(\delta)]$ for the dispersion law (III.1).

IV. CONCLUSION

We estimate the width of the energy interval corresponding to the emergence of ultra-complex conductivity diagrams for analytical dispersion relations arising in

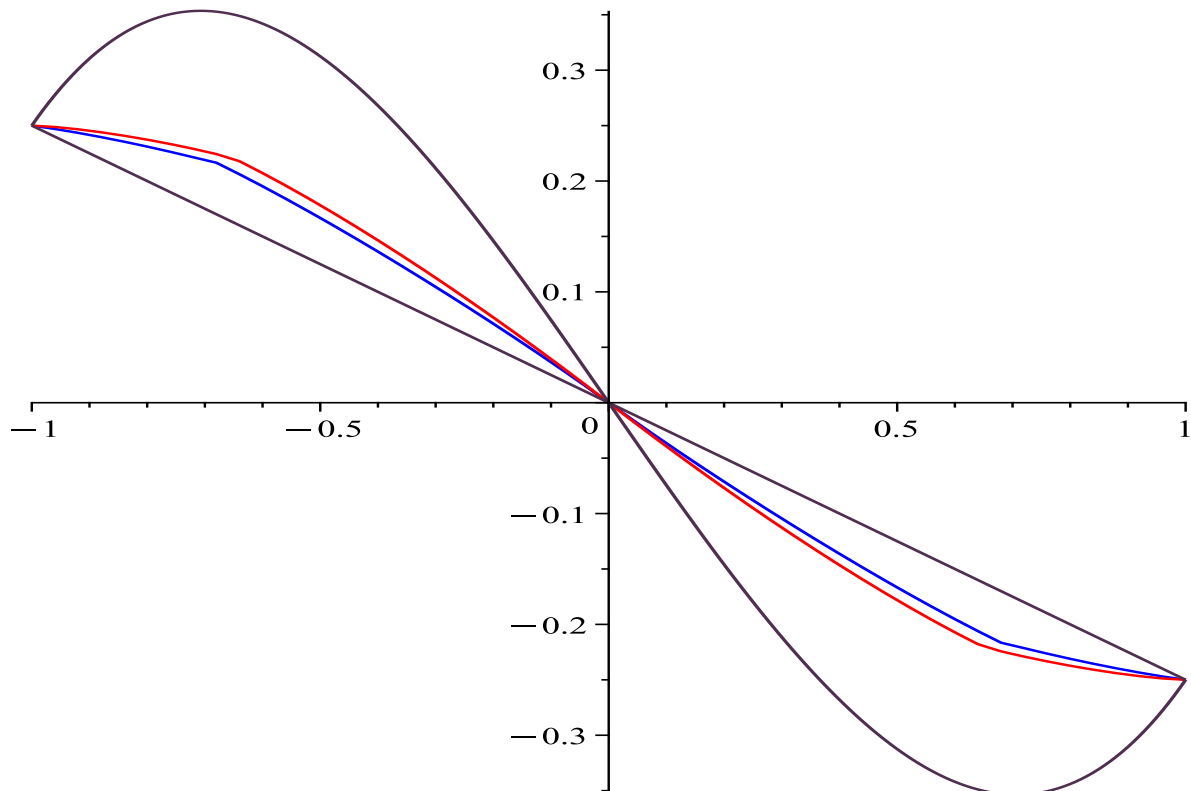


FIG. 23: Boundaries of the intervals $[\tilde{\epsilon}_0(Q, \delta), \tilde{\epsilon}_0(P, \delta)]$, $[\tilde{\epsilon}_0(P, \delta), \tilde{\epsilon}_0(Q, \delta)]$ and $(\epsilon_1^A(\delta), \epsilon_2^A(\delta))$ for the relation (III.1) in the range $-1 < \delta < 1$ (body-centered lattice).

conductors of cubic symmetry in the tight-binding approximation. The study uses higher corrections to the leading approximation in the tight-binding limit, which allows us to estimate the widths of this interval for the cases of simple and body-centered cubic lattices. The width of this interval is directly related to the probability of the occurrence of ultra-complex conductivity diagrams in materials described by the tight-binding approximation. In addition, the study of the dependence of the specified interval on the spectrum parameters also

allows us to evaluate the possibility of obtaining ultra-complex conductivity diagrams and observing the effects associated with them by means of external influence on the sample under study.

This work was supported by the Russian Science Foundation under grant no. 26-11-00292, <https://rscf.ru/project/26-11-00292/>

-
- [1] C. Kittel, Quantum Theory of Solids, Wiley, New York (1963)
 - [2] J.M. Ziman, Principles of the Theory of Solids, Cambridge University Press 1972.
 - [3] N.W. Ashcroft y N. D. Mermin, Solid State Physics, Saunders Collage Publishing, 1976.
 - [4] A.A. Abrikosov., Fundamentals of the Theory of Metals., Elsevier Science & Technology, Oxford, United Kingdom, 1988
 - [5] I.M. Lifshitz, M.Ya. Azbel, M.I. Kaganov., The Theory of Galvanomagnetic Effects in Metals., *Sov. Phys. JETP* 4:1, 41-53 (1957).
 - [6] I.M. Lifshitz, V.G. Peshansky., Galvanomagnetic characteristics of metals with open Fermi surfaces., *Sov. Phys. JETP* 8:5, 875-883 (1959).
 - [7] I.M. Lifshitz, V.G. Peshansky., Galvanomagnetic characteristics of metals with open Fermi surfaces. II., *Sov. Phys. JETP* 11:1, 131-141 (1960).
 - [8] I.M. Lifshitz, M.Ya. Azbel, M.I. Kaganov., Electron Theory of Metals. New York: Consultants Bureau, 1973.
 - [9] S.P. Novikov., The Hamiltonian formalism and a many-valued analogue of Morse theory., *Russian Math. Surveys* 37 (5), 1-56 (1982).
 - [10] A.V. Zorich., A problem of Novikov on the semiclassical

- cal motion of an electron in a uniform almost rational magnetic field., *Russian Math. Surveys* **39** (5), 287-288 (1984).
- [11] I.A. Dynnikov., Proof of S.P. Novikov’s conjecture for the case of small perturbations of rational magnetic fields., *Russian Math. Surveys* **47**:3, 172-173 (1992).
- [12] S.P. Tsarev, private communication, 1992-1993
- [13] I.A. Dynnikov., Proof of S.P. Novikov’s conjecture on the semiclassical motion of an electron., *Math. Notes* **53**:5, 495-501 (1993).
- [14] A.V. Zorich., Proc. “Geometric Study of Foliations”., (Tokyo, November 1993) / ed. T.Mizutani et al. Singapore: World Scientific, 479-498 (1994).
- [15] I.A. Dynnikov., Surfaces in 3-torus: geometry of plane sections., Proc. of ECM2, BuDA, 1996.
- [16] I.A. Dynnikov., Semiclassical motion of the electron. A proof of the Novikov conjecture in general position and counterexamples., Solitons, geometry, and topology: on the crossroad, Amer. Math. Soc. Transl. Ser. 2, 179, Amer. Math. Soc., Providence, RI, 1997, 45-73.
- [17] I.A. Dynnikov., The geometry of stability zones in Novikov’s problem on the semiclassical motion of an electron., *Russian Math. Surveys* **54**:1, 21-59 (1999).
- [18] S.P. Novikov, A.Y. Maltsev, Topological quantum characteristics observed in the investigation of the conductivity in normal metals., *JETP Letters* **63** (10), 855-860 (1996).
- [19] A.Ya. Maltsev, Anomalous behavior of the electrical conductivity tensor in strong magnetic fields., *Journal of Experimental and Theoretical Physics* **85** (5), 934-942 (1997)
- [20] S.P. Novikov, A.Y. Maltsev, Topological phenomena in normal metals, *Physics-Uspexhi* **41**:3, 231 (1998)
- [21] A. Ya. Maltsev and S. P. Novikov, Quasiperiodic functions and dynamical systems in quantum solid state physics, *Bulletin of Braz. Math. Society*, New Series **34**, 171 (2003).
- [22] A. Ya. Maltsev and S. P. Novikov, Dynamical Systems, Topology, and Conductivity in Normal Metals, *J. Stat. Phys.* **115**, 31 (2004).
- [23] R. De Leo., Topological effects in the magnetoresistance of Au and Ag., *Phys. Lett. A* **332**, 469-474 (2004)
- [24] R. De Leo., First-principles generation of stereographic maps for high-field magnetoresistance in normal metals: An application to Au and Ag., *Physica B: Condensed Matter* **362** (1-4) (2005), 62-75.
- [25] A.Ya. Maltsev, S.P. Novikov., The Theory of Closed 1-Forms, Levels of Quasiperiodic Functions and Transport Phenomena in Electron Systems., *Proceedings of the Steklov Institute of Mathematics* **302**, 279-297 (2018).
- [26] Roberto De Leo., A survey on quasiperiodic topology., Advanced Mathematical Methods in Biosciences & Applications, Springer, Eds. F. Berezovskaya and B. Toni, (2018)., arXiv:1711.01716
- [27] A.Ya. Maltsev, The second boundaries of stability zones and the angular diagrams of conductivity for metals having complicated Fermi surfaces, *Journal of Experimental and Theoretical Physics* **127** (6), 1087-1111 (2018)
- [28] A.Ya. Maltsev, The Complexity Classes of Angular Diagrams of the Metal Conductivity in Strong Magnetic Fields, *Journal of Experimental and Theoretical Physics* **129**(1), 116-138 (2019)
- [29] I.A. Dynnikov, A.Ya. Maltsev, S.P. Novikov, Geometry of quasi-periodic functions on the plane, *Russian Math. Surveys* **77** : 6, 1061-1085 (2022), arXiv:2306.11257
- [30] Anton Zorich, How do the leaves of closed 1-form wind around a surface., “Pseudoperiodic Topology”, V.I.Arnold, M.Kontsevich, A.Zorich (eds.), Translations of the AMS, Ser. 2, vol. 197, AMS, Providence, RI, 1999, 135-178.
- [31] R. De Leo., Existence and measure of ergodic leaves in Novikov’s problem on the semiclassical motion of an electron., *Russian Math. Surveys* **55**:1 (2000), 166-168.
- [32] R. De Leo., Characterization of the set of “ergodic directions” in Novikov’s problem of quasi-electron orbits in normal metals., *Russian Math. Surveys* **58**:5 (2003), 1042-1043.
- [33] R. De Leo., Topology of plane sections of periodic polyhedra with an application to the Truncated Octahedron., *Experimental Mathematics* **15**:1 (2006), 109-124.
- [34] R. De Leo, I.A. Dynnikov., An example of a fractal set of plane directions having chaotic intersections with a fixed 3-periodic surface., *Russian Math. Surveys* **62**:5 (2007), 990-992.
- [35] I.A. Dynnikov, Interval identification systems and plane sections of 3-periodic surfaces, *Proceedings of the Steklov Institute of Mathematics* **263**, 65-77 (2008).
- [36] R. De Leo, I.A. Dynnikov., Geometry of plane sections of the infinite regular skew polyhedron $\{4, 6 | 4\}$., *Geom. Dedicata* **138**:1 (2009), 51-67.
- [37] A. Skripchenko., Symmetric interval identification systems of order three., *Discrete Contin. Dyn. Sys.* **32**:2 (2012), 643-656.
- [38] A. Skripchenko., On connectedness of chaotic sections of some 3-periodic surfaces., *Ann. Glob. Anal. Geom.* **43** (2013), 253-271.
- [39] I. Dynnikov, A. Skripchenko., On typical leaves of a measured foliated 2-complex of thin type., Topology, Geometry, Integrable Systems, and Mathematical Physics: Novikov’s Seminar 2012-2014, Advances in the Mathematical Sciences., Amer. Math. Soc. Transl. Ser. 2, 234, eds. V.M. Buchstaber, B.A. Dubrovin, I.M. Krichever, Amer. Math. Soc., Providence, RI, 2014, 173-200, arXiv:1309.4884
- [40] I. Dynnikov, A. Skripchenko., Symmetric band complexes of thin type and chaotic sections which are not actually chaotic., *Trans. Moscow Math. Soc.*, Vol. 76, no. 2, 2015, 287-308.
- [41] A. Avila, P. Hubert, A. Skripchenko., Diffusion for chaotic plane sections of 3-periodic surfaces., *Inventiones mathematicae*, October 2016, Volume 206, Issue 1, pp 109-146.
- [42] A. Avila, P. Hubert, A. Skripchenko., On the Hausdorff dimension of the Rauzy gasket., *Bulletin de la societe mathematique de France*, 2016, **144** (3), pp. 539 - 568.
- [43] Ivan Dynnikov, Pascal Hubert, Alexandra Skripchenko, Dynamical Systems Around the Rauzy Gasket and Their Ergodic Properties, *International Mathematics Research*

Notices IMRN Volume 2023, Issue 8, April 2023, Pages
6461–6503

[44] A.Ya. Maltsev, On chaotic regimes of conductiv-

ity behavior in the tight-binding approximation,
arXiv:2510.17589